

Superconducting Symmetry Phases and Dominant bands in (Ca-) Intercalated AA-Bilayer Graphene

Rouhollah Gholami

Physics Department, Faculty of Science Razi University, Kermanshah, Iran
Physics Department, Faculty of Science Ilam University, Ilam, Iran

Rostam Moradian*

Physics Department, Faculty of Science Razi University, Kermanshah, Iran
Nanoscience and Nanotechnology Research Center, Razi University, Kermanshah, Iran

Sina Moradian

Department of Electrical and Computer Engineering,
University of Central Florida, Orlando FL, USA

Warren E. Pickett

Department of Physics UC Davis, One Shields Avenue, Davis CA 95616, USA
 (Dated: December 23, 2021)

Built on a realistic multiband tight binding model, mirror symmetry is used to map a calcium-intercalated bilayer graphene Hamiltonian into two independent single layer graphene-like Hamiltonians with renormalized hopping integrals (± 1 cone index). The quasiparticles exhibit two types of chirality. Here a quasi-particle consist of two electrons from opposing layers where possess an additional quantum number called “cone index” which it can be regarded as the eigenvalue of mirror symmetry operations and it play a major role in describing the physical behavior of AA-stacked bilayer graphene. To obtain tight binding parameters, both effective monolayer graphene Schrödinger equations are solved analytically and fitted to first principles band structure results. Two quasi particles (four electrons) can team up to build a Cooper pair with even or odd chirality. Treatment of the pairing Hamiltonian leads to two decoupled gap equations for each of these effective graphene monolayer sectors that means pairing of quasi-particles with different cone index is forbidden. The decoupled gap equations are solved analytically to obtain all the possible order parameters for superconducting phases. Two nearly “flat bands” crossing the Fermi energy, each related to the graphene-like structures, are responsible for two distinct superconductivity gaps that emerge. Depending on how much these bands are affected by the intercalant and which is closer to the Fermi energy, distorted *s*-wave or *d*-wave superconductivity may become dominant. Numerical calculations reveal that *d*-wave superconductivity is dominant in both sectors. For these two dominant phases we present the relation of the pairing potential to the superconducting critical temperature T_c . Within the range of 0-6 K which superconductivity has been observed experimentally, transition from single-gap to dual-gap superconductivity is possible. Adopting the two gap viewpoint of superconductivity in C_6CaC_6 , the dominant *d*-wave states should have the same critical temperature. Around $T_c = 2K$ these two relations intersect, otherwise superconductivity has been realized just in the one of these two sectors and disappear in the other one. In this case, the superconducting coexistence with the Dirac electrons is possible.

I. INTRODUCTION

Discovery of new superconducting phases, often at low temperature, has been one of the active achievements in recent decades, sometimes overshadowed by the high profile effort to push toward higher temperature superconductors. Remarkable progress in the synthesis or fabrication of nanostructures in the recent years is opening new horizons in engineering the physical properties of new classes of materials. Two dimensional (2D) phases, including superconducting ones,^{1,2} received renewed attention from the discovery that monolayer graphene can be peeled off, and subsequently found that it can be synthesized from the gas phase. Dirac (charge neutrality) points, has become of rising interest. While graphene, with its massless Dirac points, hosts many unusual quantum properties with potential applications, pristine graphene does not support superconductivity due to its vanishing density of states (DOS) at the Dirac points.

Despite that, discussion of superconductivity in doped graphene has been profuse with theoretical models³⁻⁸. With the many pictures raising various possibilities (such as chiral *d+id* pairing³⁻⁵, coexistence of both chiral *d+id* and *f*-wave⁷ and *p+ip*⁸,) but little of a certain nature. However, superconductivity in lithium decorated graphene around 6K was predicted theoretically⁹ and subsequently reported experimentally.¹⁰ Graphite intercalation compound (GIC) superconductors have been known and studied for decades.¹¹ Recent advances in few layer graphene (FLG) fabrication

methods have caused theoretical attention to their electronic physics. Due to its strong two dimensionality, bilayer graphene (BIG) has provided an attractive platform for studying 2D electron correlation effects.¹⁴ Because of the weak interlayer van der Waals forces, the layers of the graphene bilayer can rotate relative to each other and form different ordering stakes *i.e.* AA, AB (Bernal phase), or even “twisted bilayer” form.

Following the indication of a Mott insulating phase in twisted bi-layered graphene¹⁸ and the observation of superconductivity upon doping,¹⁹ these types of systems have revived interest and may realize a new class of superconductor. It seems that bilayer graphene can host superconductivity, magnetism, and other unusual phases. In addition to relativistic character of quasi particles in single layer graphene, interlayer coupling causes the bilayer graphene to exhibit behaviors that are not observed in the single layer graphene. Most fascinating behaviors of TBIG are played by interlayer hybridization of nearby Dirac K points of opposite layers via interlayer tunneling in a spatially periodic way²⁰. Interlayer coupling causes quasi particles in the AB-stacked bilayer graphene behave as massive chiral quasi-particle with parabolic dispersion near the Dirac Fermi points. In this manuscript we will see that quasi-particles in AA-stacked BIG can exhibit extra aspects of such behaviors.

Beside TBIG, when the electron-electron correlations effects are taken into consideration in AA and AB-stacking structures, theory suggests a variety of instabilities with potential technological applications, including unusual quantum Hall effects, antiferromagnetic phases, and tunable band gap opening at the charge neutral points (for a review see [14]), some of which have been confirmed experimentally.²⁶ Although it is difficult to distinguish AA-stacked BIG from single layer graphene but Some authors claimed to fabricate AA-BIG experimentally. However, it has been received much less attention than more stable AB-stacked phase. Unlike Fermi points in monolayer graphene and AB-stacked, the well nested Fermi surface of pristine AA-BIG consists of small electron and hole pockets of equal area. This feature has drastic consequences, tending the system toward electron instabilities such as antiferromagnetism at zero doping and bilayer exciton condensation when doped.^{14,30-33}

Superconducting instabilities in doped or gated AB-stacking phases have been predicted. An effective two-band Hamiltonian with attractive interactions was used in Ref²⁷ to investigate the possibility of a time reversal breaking $d + id$ phase in moderately doped AB-stacked BIG. Using a weak-coupling renormalization group formalism, the possibility of unconventional superconducting orders from repulsive interaction on doped AB-stacked honeycomb bilayer in d -wave, f -wave, and pair density wave channels were discussed in by James *et al.*²⁸ Spin triplet s -wave pairing could also arise.²⁹ Superconductivity reported in Ca-intercalated bilayer graphene represents the thinnest limit of graphite intercalation compounds (GICs)²², at 4K²⁴ and around 6.4K in Ca-doped graphene laminates²⁵. Even so, the superconducting phase of AA-graphene has been addressed very little in the literatures very rarely.

Based on an effective Hamiltonian with an attractive potential between inter- and intra-layer near neighbor sublattices Alidoust *et al.*³⁴ to study phonon-mediated superconducting pairing symmetries that may arise in AA, AB (and AC)-stacking bilayer graphene at the charge neutral point and beyond (by varying chemical potential). They claimed that at a finite doping, AB stacking can develop singlet and triplet d -wave symmetry beside s -wave, p -wave and f -wave that can be achieved at the charge neutral point, while the AA-stacked phase, similar to the undoped case, is unable to accept d -wave pairing.

Motivated by experimental observation of superconductivity in Ca doped bilayer graphene, a more realistic model has been introduced here to obtain all possible superconducting symmetries which can be arise analytically. In this manuscript, we follow the notion that Calcium doped bilayer graphene as mentioned in the ref.²² as the thinnest limit of graphite intercalation compounds for which the structure Consists of Ca intercalated bilayer AA- stacked graphene (Fig.1(a)). However, recently, another possibility has been raised experimentally³⁷.

Based on mean-field treatment of an extended Hubbard model, a realistic tight-binding model has been used where its parameters are determined by a fitting to DFT band structure. By adding an effective attractive interactions between interlayer and intralayer electrons, all possible superconductivity pairing symmetry characters of C_6CaC_6 has been studied in details (which can be applied to any related graphene-like structures such as $B_3N_3CaB_3N_3$). We will take advantage of the observation that, mathematically one can use mirror symmetry properties of Bloch coefficients of intercalated AA -stacked bilayer graphene and interpret their Hamiltonian as two independent single layer pseudo-graphene structures (even and odd sectors) where one of them (even symmetry sector) is decorated with calcium layer. This notion leads to the emergence of a topological number called cone index ($c = \pm 1$). Conservation of cone index during Klein tunneling across an n-p junction is one of the interesting unique behaviors in AA-stacked bilayer where it raises the possibility of cone-tronic devices based on AA-BIG.³⁸

In the real space a quasi-particle consist of two electrons from opposing layers with the same symmetrical position where they possess an additional quantum cone index beside their chirality nature near the Dirac points. The cone index concept is a unique feature in describing quasi-particles behaviors in AA-BIG with respect to single layer graphene. Two quasi particles (*i.e.* “four electrons”) can team up to build a Cooper pair as one can see in Fig. 1(b,c). We will see that only quasiparticles with the same cone index can be paired.

It will be shown that the question of superconducting phases in metal-intercalated bilayer graphene such as C_6CaC_6 can be decoupled to two independent gap equations corresponding to each of the even and odd sectors which they can

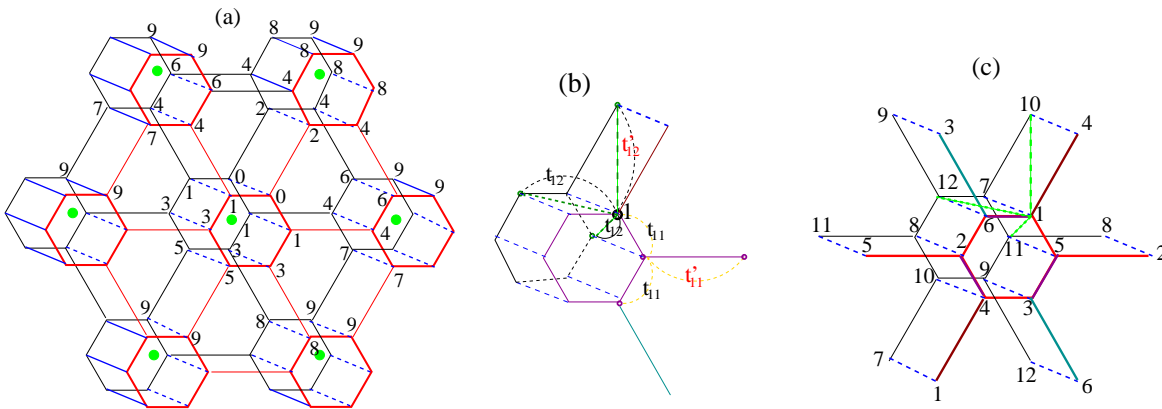


FIG. 1: Structure and notation. **(a)** Sketch (exaggerated) of shrunk bilayer graphene where numbers indicate C-C first, second, and so on, neighbors of reference carbon atom in each layer. **(b)** Shows the unit cell of intercalated bilayer graphene. In this Kekulé structure the intralayer hopping energies symmetry between first nearest neighbor atoms is broken. Intralayer hopping parameters along hexagonal bonds are the same and shown by t_{11} while between the long bond slightly has been changed given by t'_{11} . Similarly interlayer hopping are given by t_{12} and t'_{12} . Symmetry breaking of hopping energies leads to open two unequal gap at the Dirac points that folded back to the Γ point. **(c)** Intra-plane superconductor pairing amplitudes ($\Sigma_1 \Sigma_2 \Sigma_3$) are between 1-4, 3-6 and 2-5 subsites respectively, ($\Delta_1 \Delta_2 \Delta_3$) are between 3-5, 2-4 and 1-6 subsites respectively, and ($\Pi_1 \Pi_2 \Pi_3$) are between 2-6, 1-5 and 3-4 subsites respectively. Also, inter-plane superconductor pairing amplitudes ($\Sigma'_1 \Sigma'_2 \Sigma'_3$) are between 1-10, 3-12 and 2-11 subsites respectively, ($\Delta'_1 \Delta'_2 \Delta'_3$) are between 3-11, 2-10 and 1-12 subsites respectively, and ($\Pi'_1 \Pi'_2 \Pi'_3$) are between 2-12, 1-11 and 3-10 subsites respectively.

be solved analytically (or nearly so) to obtain all possible pairing symmetry phases which can be probed experimentally.

The two gap nature of superconductivity that is one of the unique feature of MgB₂³⁹ can be inspected here similarly. We have numerically predicted that in the temperature range of 0-6 K the phase transition from d-wave single-gap to dual-gap d-wave superconductivity could be observed. Using *ab initio* anisotropic Migdal-Eliashberg theory including Coulomb interaction, Margine *et al.*⁴⁰ concluded that C₆CaC₆ should support phonon mediated superconductivity with a critical temperature $T_c = 6 - 7\text{K}$, within the range of observations, and it exhibits two distinct superconducting gaps on the electron and hole Fermi surface pockets which is in agreement with the result has been obtained in the present manuscript.

The rest organization of the paper is as follows. Section II introduces the model Hamiltonian that we study, with Sec. III setting the stage by obtaining mostly analytic diagonalization of the non-interacting system. In Sec. IV, the treatment of pairing and presentation of superconducting phases is presented. In Sec. V, analytic insight are complemented by numerical solutions, followed by a discussion and summary in Sec. VI. Many of the analytic expressions are delegated to Appendices.

II. MODEL HAMILTONIAN

The system we consider, illustrated in Fig.1(a), consists of AA stacked bilayer graphene intercalated by Ca metal layer in which intercalant atoms are located on the central symmetry plane of bilayer graphene at the center of neighboring carbon hexagons. The distance between the graphene layers is calculated to be $h = 4.63\text{\AA}$ in the case of Ca intercalation. The nearest in-plane Ca-Ca distance is $\xi = 4.26\text{\AA}$. Charge transfer from Ca to the graphene layers leads to breaking symmetries of hopping amplitudes, and of C-C bond lengths similarly to those of Li decorated monolayer graphene^[41]. The attractive interaction between metal cations and C atoms after charge transfer contracts the Ca-C distance and reduces the C-C bond lengths in the Ca-centered hexagon to $a_1 = 1.419\text{\AA}$. As a result the bond length of neighboring C atoms in different hexagons is somewhat larger, at $a_2 = 1.423\text{\AA}$. Also in this “shrunk bilayer graphene”⁴¹ the hopping integrals between short-bond inter- and intra-layer carbons are respectively t_1^{11} and t_1^{12} , while those between stretched carbon sites will be denoted $t_1^{\prime 11}$ and $t_1^{\prime 12}$. The lattice then becomes a two dimensional hexagonal Bravais lattice with thirteen atomic sites. The sites of i -th cell will be labeled as $A_{i1}^m, A_{i2}^m, A_{i3}^m, B_{i1}^m, B_{i2}^m, B_{i3}^m$ and Ca , where m is layer index and takes $m = 1, 2$.

The Hamiltonian of this system is

$$\hat{H} = - \sum_{i\alpha} \sum_{j\beta, \sigma} t_{i\alpha, j\beta}^{\sigma, \sigma} \hat{c}_{i\alpha\sigma}^\dagger \hat{c}_{j\beta\sigma} + \sum_{i\alpha, \sigma} (\epsilon_{i\alpha} - \mu_o) \hat{n}_{i\alpha\sigma} + \frac{1}{2} \sum_{i\alpha, \sigma} \sum_{j\beta, \sigma'} U_{i\alpha, j\beta}^{\sigma, \sigma'} \hat{n}_{i\alpha\sigma} \hat{n}_{j\beta\sigma'} = \hat{H}_N + \hat{H}_P. \quad (1)$$

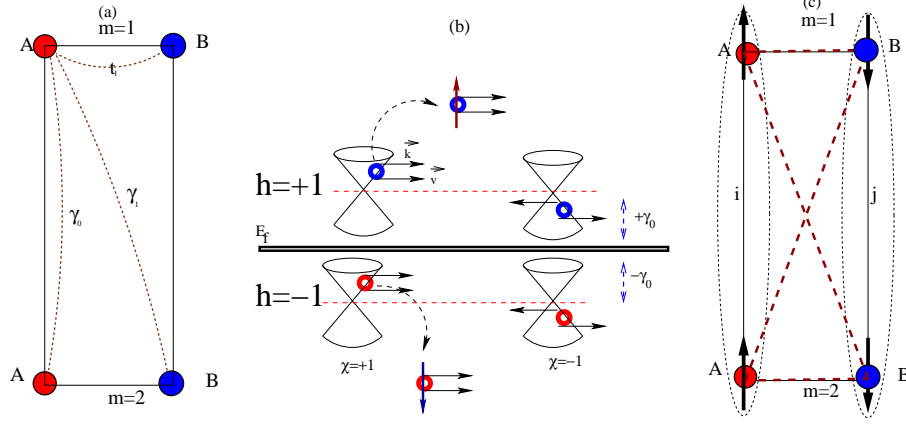


FIG. 2: Structure and notation. (a) Shows AA-stacked BIG unit cell, $m=1,2$ indicate layer index, t_1 and γ_1 are nearest neighbor intralayer and interlayer hopping energies respectively and γ_0 is direct interlayer hopping. (b) Near the Dirac points K & K' ($K'=-K$) the even and odd sector of pristine AA-BIG are shown by γ_0 -up and down shifted Dirac Cones. Quasi-particles in even sector (odd sector) are shown by blue (red) circles. χ shows v -chirality while h is the index of h -chirality (c) shows a Cooper pair. Up and down pseudo-spin (h -Pspin) of irreducible blocks of AA-BIG Hamiltonian viz. H^+ and H^- are shown by dashed ellipses i & j . Here a quasi-particle consists of two electrons with the same spin which each one located at similar sub-sites in the opposing layers. These quasi-particles describe by an additional h -chirality index. Two quasi particles (i.e. “four electrons”) can team up to build a Cooper pair as one can see in Fig. 1(b,c). We will see that only quasiparticles with the same cone index can be paired

where α and β run over the sublattice orbitals $A_i^m p_z$, $B_i^m p_z$ and Ca s . Here $\hat{c}_{i\alpha\sigma}^\dagger$, $\hat{c}_{i\alpha\sigma}$ are creation and annihilation operators of an electron with spin σ on subsite α of i th lattice site, and $\hat{n}_{i\sigma} = \hat{c}_{i\sigma}^\dagger \hat{c}_{i\sigma}$ is the electron number operator. The chemical potential is μ_0 and $t_{i\alpha,j\beta}$ is the hopping integral from α subsite of i th site to the β subsite of j th site. Here U is an effective negative interaction between electrons in the extended (negative U) Hubbard model that allows the possibility of superconductivity.

III. THE NON-INTERACTING SYSTEM

In this section a thirteen band tight binding model, consisting of twelve p_z C orbitals and the Ca s orbital, for Ca-intercalated bilayer graphene is constructed, to be applied to study superconducting states of this system within BdG theory. The non-interacting system Hamiltonian is invariant under mirror symmetry, which leads to division of the intercalated AA-BIG band structure into two sectors characterized by eigenvalues of mirror operation. Here we take advantage of the mirror symmetry. We first apply this reduction to the simple case of pristine AA-BIG.

A. Reducible Tight Binding Model for Pristine AA-staked Bilayer Graphene

The unit cell of AA-BIG, illustrated in Fig. 2(a), consists of four atoms A_1 , B_1 in the top layer and A_2 , B_2 in the bottom layer. The Schrödinger equation for this system in terms of Bloch coefficients is given by

$$\left[\begin{array}{c|c} H_{11} & H_{12} \\ \hline H_{21} & H_{22} \end{array} \right] \begin{pmatrix} \chi_1 \\ \chi_2 \end{pmatrix} = E_n \begin{pmatrix} \chi_1 \\ \chi_2 \end{pmatrix}, \quad \begin{pmatrix} \chi_1 \\ \chi_2 \end{pmatrix} = \begin{pmatrix} \mathcal{C}_{A_1}(\vec{k}) \\ \mathcal{C}_{B_1}(\vec{k}) \\ \mathcal{C}_{A_2}(\vec{k}) \\ \mathcal{C}_{B_2}(\vec{k}) \end{pmatrix} \quad (2)$$

where 2×1 column matrices χ_1 and χ_2 are components of AA-BIG iso-spinors, $H_{11} = H_{22}$ and $H_{12} = H_{21}$ are intralayer and interlayer hopping matrix respectively. The 4-component “Dirac spinor” (Dirac representation) is reducible. Using the unitary transformation $U = \frac{1}{\sqrt{2}} \begin{pmatrix} I_2 & I_2 \\ I_2 & -I_2 \end{pmatrix}$, it decomposes into two irreducible representations, acting only on two 2-component right and left hand “Weyl spinors.” Similar transformations decouple the 4-component iso-spinor of AA-BIG into two 2-component chiral iso-spinors. This connection is an pedagogically useful mathematical similarity

between the Schrödinger equation of AA-BIG and the Dirac equation, because it can give a insight into the prediction of quasiparticle behavior in AA-BIG in analogy with relativistic particles such as neutrinos. Mirror symmetry leads to

$$\mathcal{C}_{A_1}(\vec{k}) = \pm \mathcal{C}_{A_2}(\vec{k}), \quad \mathcal{C}_{B_1}(\vec{k}) = \pm \mathcal{C}_{B_2}(\vec{k}) \quad (3)$$

Inserting Eq. 3 into Eq. 2 and defining new single layer graphene-like Hamiltonians $H^\pm = H_{11} \pm H_{12}$, the four band Schrödinger equation converts into two decoupled single layer graphene two band Schrödinger equations of the form

$$H^+ \chi_R = E_n^+ \chi_R, \quad H^- \chi_L = E_n^- \chi_L, \quad (4)$$

wherein 2-component iso-spinors (has been shown in Fig. 2c) are given by

$$\chi_R = \frac{1}{\sqrt{2}}(\chi_1 + \chi_2) = \begin{pmatrix} \mathcal{C}_A^+(\vec{k}) \\ \mathcal{C}_B^+(\vec{k}) \end{pmatrix}, \quad \chi_L = \frac{1}{\sqrt{2}}(\chi_1 - \chi_2) = \begin{pmatrix} \mathcal{C}_A^-(\vec{k}) \\ \mathcal{C}_B^-(\vec{k}) \end{pmatrix}. \quad (5)$$

The \pm sign appearing in the even and odd sector Hamiltonians are the $h = \pm 1$ eigenvalues of the mirror symmetry operator $\hat{S}_h = \begin{pmatrix} 0 & I_2 \\ I_2 & 0 \end{pmatrix}$ which is the same as fifth Dirac gamma matrix $\hat{\gamma}^5$ that reflects the right (χ_R) or left hand (χ_L) chirality of quasiparticles in the relativistic quantum field theory. This additional \pm topological index called by Sanderson and Ang (AS) as ‘‘cone index.’’³⁸. SA have shown that quasiparticles in AA-BIG are not only chiral but are also characterized by ‘‘cone index.’’ So we will refer to the cone index as h-chirality index and to usual helicity appears again as v-chirality. According to this notion, one can describe Dirac cones in AA-BIG shown in the Fig. 2(b) with two kind of chirality with respect to asymmetric in such a way that the structure and its vertical (‘‘**v-chirality**’’) and horizontal (‘‘**h-chirality**’’) mirror image are not superimposable. This chirality is a general aspect of AA-BIG quasi-particles that holds for general hoppings and over the entire Brillouin zone. SA show that electron transport across a barrier must conserve the cone index, a consequence of the Klein tunneling behavior in AA-stacked BIG. In the following sections we will extend the consequence of the cone index notion to superconductivity pairing.

A quasi-particle in the even sector (odd sector) consists of two electron ($2e$ charge) from opposing layers with the same spatial symmetry which possess $h = +1$ (-1) cone index and on-site energy of $\varepsilon^+ = +\gamma_0$ ($-\gamma_0$) respectively. Hopping of a quasi-particle from A subsite to nearest neighbor B subsite in the even-sector (odd-sector) changes the energy by $t^+ = t_1 + \gamma_1$ ($t^- = t_1 - \gamma_1$). This decoupling is more than just a simple mathematical diagonalization and symmetry characterization. One can interpret the Hamiltonian of AA-BIG as a single layer honeycomb lattice Hamiltonian with two types of charge carriers described by

$$H = - \sum_{i,j} \sum_{\sigma=\pm} t_{i,j}^\sigma a_{i\sigma}^\dagger b_{j\sigma} + \sum_{i\sigma} \varepsilon^\sigma (a_{i\sigma}^\dagger a_{i\sigma} + b_{i\sigma}^\dagger b_{i\sigma}) + h.c$$

where $a_{i\sigma}^{\pm\dagger}$ ($b_{i\sigma}^{\pm\dagger}$) is the creation operator of a quasiparticle in the A(B) subsite of the i th site with $\sigma = \pm 1$ wherein σ represents h-chiral Pseudo-spin (h-Pspin). where $a_{i\sigma}^{\pm\dagger}$ ($b_{i\sigma}^{\pm\dagger}$) is the creation operator of a quasiparticle in the A(B) subsite of the i th site with $\sigma = \pm 1$ wherein σ represents h -chiral Pseudo-spin (h -Pspin).

In the intralayer and interlayer nearest neighbor hopping approximation, viz. t_1 , γ_0 and γ_1 the system Hamiltonian is given by

$$\begin{bmatrix} H_{11} & H_{12} \\ H_{12} & H_{11} \end{bmatrix} \approx - \begin{bmatrix} \mu & t_1 f(\vec{k}) & \gamma_0 & \gamma_1 f(\vec{k}) \\ t_1 f^*(\vec{k}) & \mu & \gamma_1 f^*(\vec{k}) & \gamma_0 \\ \gamma_0 & \gamma_1 f(\vec{k}) & \mu & t_1 f(\vec{k}) \\ \gamma_1 f^*(\vec{k}) & \gamma_0 & t_1 f^*(\vec{k}) & \mu \end{bmatrix}; \quad H^\pm = H_{11} \pm H_{12} = - \begin{bmatrix} \mu \pm \gamma_0 & t^\pm f(\vec{k}) \\ t^\pm f^*(\vec{k}) & \mu \pm \gamma_0 \end{bmatrix} \quad (6)$$

Here $t^\pm = t_1 \pm \gamma_1$ and t_1 (γ_1) is the nearest neighbor intralayer(interlayer) hopping between A and B sublattices and the direct interlayer hopping (i.e. A_1 to A_2 or B_1 to B_2) is given by γ_0 . Here μ is chemical potential, also $f(\vec{k}) = \sum_{i=1}^3 e^{i\vec{k}\cdot\vec{\delta}_i}$ wherein $\vec{\delta}_i$ vectors connect A subsite to three in-plane nearest neighbor B subsites.

The decoupled Schrödinger equation Eq. 4 has eigenvalues

$$E_n^\pm(\vec{k}) = \mu + \eta_{v-c}(t^\pm |f(\vec{k})|) \pm \gamma_0 \quad (7)$$

where $\eta_{v-c} = \pm 1$. The four bands of AA-BIG separates into two independent up-down shifted single layer graphene bands where they are referred to as the even and odd sector, respectively.

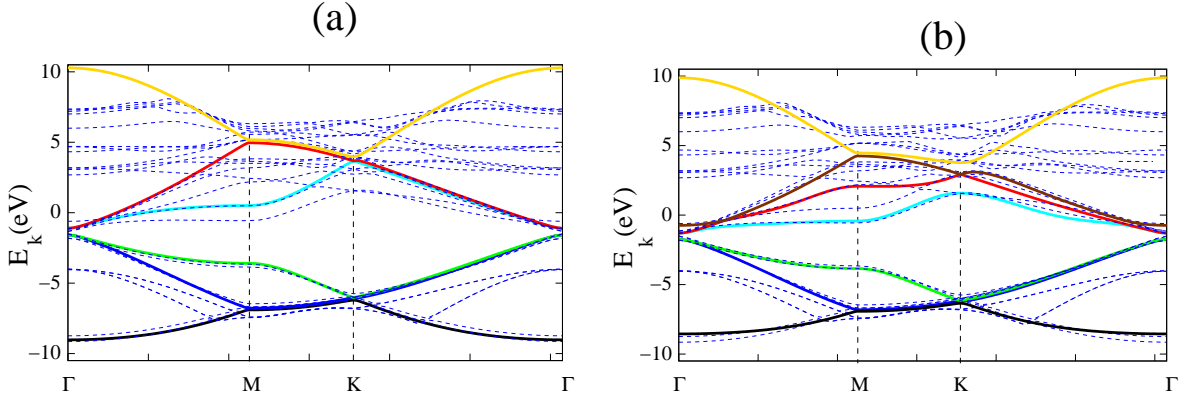


FIG. 3: Band structure of C_6CaC_6 . Left panel: bands emphasizing the six pseudo-graphene layer bands ($H^-(\vec{k})$). Right panel: emphasis on the seven pseudo-graphene layer bands ($H^+(\vec{k})$). Thin dashed lines indicate the DFT bands, while the fitted bands are shown in color.

Near the Dirac points, the dispersion energies $E_n^\pm(\vec{k}) = \hbar v_f^\pm |\vec{k}| \pm \gamma_0$ of odd and even sectors are shown by two up-down shifted Dirac cones in Fig. 2(b) where $v_f^\pm = \frac{\sqrt{3}t^\pm a}{2\hbar}$ is Fermi velocity of $h = \pm 1$ quasi particles. Generalizing the tight binding model to include further neighbor hopping terms can highlight some hidden aspects of the AA-stacked Dirac cone quasi-particles. For second neighbor interlayer hopping, γ_1 taken into regard one can distinguish quasi-particles with the same chirality (v-chirality) and different cone index (h-chirality) from their velocities which could be inspected experimentally. The Fermi velocity of Dirac cone with $h = -1$ chirality decreases as interlayer hopping increases, while the velocity of $h = +1$ quasi-particle increases:

$$v_f^+ - v_f^- = \frac{\sqrt{3}a}{\hbar} \gamma_1.$$

In the strong inter layer coupling $t_1 \rightarrow (-)\gamma_1$ Fermi velocity $v_f^-(v_f^+) \rightarrow 0$ and odd(even) sector bandwidth tends to zero. As shown in the next subsection, interlayer coupling γ_1 may be considerable, so that inequality could be considerable.

B. Analytic Tight Binding Model for Intercalated Bilayer Graphene

In this subsection we will generalize the previous procedures to include the case of experimentally observed structures such as Li or Ca intercalated bilayer graphene. We will follow the notion it believe that these structure are intercalated AA-stacked bilayer graphene as has been shown in the Fig. 1. From the beginning, the Hamiltonian is generalized to incorporate several broken symmetries, including the on-site energies, hopping integrals, and bonds lengths (geometry). Due to this generalization, it can be used to obtain analytic dispersion energies of not only C_6CaC_6 , but also related graphene-like structures such as $B_3N_3CaB_3N_3$. The Hamiltonian of such a non-interacting system is

$$\hat{H}_N = - \sum_{i\alpha} \sum_{j\beta, \sigma} t_{i\alpha, j\beta}^{\sigma, \sigma} c_{i\alpha\sigma}^\dagger c_{j\beta\sigma} + \sum_{i\alpha, \sigma} (\epsilon_{i\alpha} - \mu_o) \hat{n}_{i\alpha\sigma}. \quad (8)$$

where α and β run over sublattice orbitals A_i^m , B_i^m and the intercalated atom (e.g. Ca) orbital. The Schrödinger equation for this system in terms of Bloch coefficients in \vec{k} space becomes

$$\sum_{\beta=0}^{12} \epsilon_{\alpha\beta}(\vec{k}) \mathcal{C}_\beta + (\epsilon_\alpha - \mu_o) \mathcal{C}_\alpha = E(\vec{k}) \mathcal{C}_\alpha \quad \text{where} \quad \epsilon_{\alpha\beta}(\vec{k}) = -\frac{1}{N} \sum_{ij} e^{i\vec{k} \cdot (\vec{r}_{i\alpha} - \vec{r}_{j\beta})} t_{i\alpha j\beta}^{\sigma\sigma}. \quad (9)$$

Here the $\beta=0, 1, 2, \dots, 12$ subscripts refer respectively to intercalant Ca, $A_1^1, A_2^1, A_3^1, B_1^1, B_2^1, B_3^1, A_1^2, A_2^2, A_3^2, B_1^2, B_2^2$ & B_3^2 and N is the number of unit cells. Here $\epsilon_{A_i} = \epsilon_A$ and $\epsilon_{B_i} = \epsilon_B$.

Mirror symmetry of this system result in the relations

$$\mathcal{C}_\alpha(\vec{k}) = \pm \mathcal{C}_{\alpha+6}(\vec{k}), \quad \alpha = 1, 2, \dots, 6 \quad (10)$$

which reflects the mirror symmetry through the Ca plane that separates even and odd states (i.e. $h = \pm 1$ h-chirality). By inserting Eq. 10 into Eq. 9, with more detail given in Appendix A, one obtains two independent Schrödinger equations corresponding to eigenvectors $\Psi_i^-(\vec{k})^T = (0, \mathcal{C}_i(\vec{k}), -\mathcal{C}_i(\vec{k}))$, $\Psi_j^+(\vec{k})^T = (\mathcal{C}_0(\vec{k}), \mathcal{C}_j(\vec{k}), +\mathcal{C}_j(\vec{k}))$ respectively. For the odd eigensystem, the Schrödinger Eq.35 reduces to following 6×6 matrix eigenvalue problem

$$H^-(\vec{k})\mathcal{C}_n(\vec{k}) = (H_{11} - H_{12})\mathcal{C}_n(\vec{k}) = E_n^-\mathcal{C}_n(\vec{k}), \quad n = 1, 2, \dots, 6. \quad (11)$$

The Schrödinger Eq. 11 can be solved analytically, with the six eigenvalues presented in Appendix I, Eq. 51. These expressions are unaffected by the intercalant layer due to the separation of even and odd mirror symmetries, but the presence of Ca will renormalize parameters. For the even mirror sector, the Schrödinger equation Eq.35 reduces to the following 7×7 matrix eigenvalue problem

$$H_c^+(\vec{k}) \begin{pmatrix} \mathcal{C}_0(\vec{k}) \\ \sqrt{2}\mathcal{C}_n(\vec{k}) \end{pmatrix} = \begin{bmatrix} h_0(\vec{k}) & \sqrt{2}h_{01}(\vec{k}) \\ \sqrt{2}h_{10}(\vec{k}) & H^+(\vec{k}) \end{bmatrix} \begin{pmatrix} \mathcal{C}_0(\vec{k}) \\ \sqrt{2}\mathcal{C}_n(\vec{k}) \end{pmatrix} = E_n^+ \begin{pmatrix} \mathcal{C}_0(\vec{k}) \\ \sqrt{2}\mathcal{C}_n(\vec{k}) \end{pmatrix}, \quad (12)$$

where $n = 7, \dots, 13$. The other seven bands of the Schrödinger equation Eq. 35 can be obtained from solving the new Schrödinger Eq. 12. The k-dependent part of corresponding matrix components of H_{11} and H_{12} are identical in form, differing only in hopping parameters, hence $H^\pm(\vec{k})$ can be considered as a shrunken graphene monolayer Hamiltonian with renormalized hopping parameters. It follows that, Similar to the pristine bilayer graphene (see¹⁴), intercalated bilayer graphene can be interpreted as two independent pseudo-graphene monolayers where one of them is dressed by a modified hopping Ca layer. The thirteen bands of bilayer graphene divide into two groups, six bands group (odd symmetries) corresponding to H^- Hamiltonian and seven bands group (even symmetries) which are eigenvalues of H_c^+ matrix.

Mathematically many of the results obtained in ref. [41] can be generalized to these graphene like structures but with renormalized hopping parameters. For general \vec{k} , except at Γ , it is challenging to obtain an exact analytical solution of the Schrödinger equations of Eq. 12. At the graphene Dirac points which have become folded back to the this supercell Γ point, symmetry breaking of nearest neighbor intra- and interlayer hopping parameters i.e. t_{11} , t'_{11} and t_{12} , t'_{12} (Fig. 1b) results in two unequal small gaps with different centers, corresponding to six (odd-sector) and seven (even-sector) band pseudo-graphene Hamiltonians, given by

$$E_g^+ = 2|t_1^+ - t_1'^+|, \quad E_g^- = 2|t_1^- - t_1'^-| \quad (13)$$

where $t_1^\pm = t_{11} \pm t_{12}$ and $t_1'^\pm = t'_{11} \pm t'_{12}$. For the use of graphene as field effect transistors, it is necessary to create a tunable gap. Tunable and sizable band gap can be constructed in single layer[?] by decoration and in the bilayer graphpe by intercalation as can be seen from Eq. 13.

The effect of symmetry braking of the the inter-layer coupling parameter i.e. $\Delta\gamma_1 = t_{12} - t'_{12}$ leads to inequality of even and odd sector gaps. Knowing the size of these energy gaps, one can find the difference in the first nearest neighbor intra and inter-layer hopping parameters symmetry breaking (suppose $\Delta t > 0$, $\Delta\gamma_1 > 0$ and $\Delta t > \Delta\gamma_1$),

$$E_g^+ - E_g^- = 4\Delta\gamma_1, \quad E_g^+ + E_g^- = 4\Delta t \quad (14)$$

where $\Delta t = t_{11} - t'_{11}$. These two gaps are characteristic of AA-IBIG. In the case of Li- intercalated BIG, experimental ARPES spectra (Fig. 4 Ref.²³) shows two distinct gaps of wide $E_g^- = 0.20eV$ and $E_g^+ = 0.46eV$. In this reference the authors has equated the ratio of these two gaps as the ratio of the interlayer skew coupling parameters (γ_2 and γ_2' in their notation). Equation 14 slightly correct the discussion that has been stated in the [Sec. III, sub-sec.C of Ref.²³] about this ratio.

Eq. 12 results in the event that intercalant layer hopping parameters to graphene sheets are negligible, as in the case of Li-decorated graphene where Li atoms fully ionize and the Li-associate band lies above the Fermi energy, so Li-C hopping effects are negligible. In this particular case the odd (-) and the even (+) nontrivial eigenvalues of H^\pm matrix, are given by

$$E_{sh;m,l}^\pm(t_i, \vec{\xi}_i, \vec{k}) = \mu_m^\pm(\vec{k}) - \mu_o + \frac{1}{2} \left[\varepsilon_A + \varepsilon_B + (-1)^l \sqrt{(\varepsilon_A - \varepsilon_B)^2 + 4w_m^\pm(t_i, \vec{\xi}_i, \vec{k})} \right], \quad m = 1, 2, 3; l = 1, 2 \quad (15)$$

wherein $\mu_m^\pm(\vec{k})$, $w_m^\pm(t_i, \vec{\xi}_i, \vec{k})$ are defined in Eqs. 52 and 55 respectively. Details for obtaining these results are presented in Appendix A and ref. [41].

Now further notation is established. Similar to the case of pristine AA-BIG investigated in the previous subsection, this transformation recast the noninteracting Hamiltonian Eq. 8 as the direct sum of two single layer pseudo-graphene

structures with renormalized hopping integrals in the right and left hand chiral representation of the form

$$\hat{H}_N = \hat{H}_N^+ \oplus \hat{H}_N^- = \sum_{ij\sigma} \sum_{\alpha,\beta=0}^6 t_{i\alpha\sigma,j\beta\sigma}^+ \hat{c}_{i\alpha\sigma}^{+\dagger} \hat{c}_{j\beta\sigma}^+ \oplus \sum_{ij\sigma} \sum_{\alpha,\beta=1}^6 t_{i\alpha\sigma,j\beta\sigma}^- \hat{c}_{i\alpha\sigma}^{-\dagger} \hat{c}_{j\beta\sigma}^- \quad (16)$$

wherein, as illustrated in the Fig.2(c), we introduced quasiparticle creation operators and hopping integrals in real space,

$$\hat{c}_{i\alpha\sigma}^{(\pm)\dagger} = \frac{1}{\sqrt{2}}(\hat{c}_{i\alpha\sigma}^\dagger \pm \hat{c}_{i,\alpha+6,\sigma}^\dagger), \quad t_{i\alpha\sigma,j\beta\sigma}^\pm = t_{i\alpha\sigma,j\beta\sigma}^{inter} \pm t_{i\alpha\sigma,j\beta+6\sigma}^{intra}, \quad \alpha, \beta = 1, \dots, 6. \quad (17)$$

The creation operator $\hat{c}_{i\alpha\sigma}^{(\pm)\dagger}$ creates an quasi-particle with $h = \pm 1$ h-chirality and spin (σ) at $i\alpha$ atomic subsite of each of these two graphene-like structures, participate directly in the formation of superconducting phases.

The separation of thirteen bands of intercalated bilayer graphene into groups of six bands with odd-symmetry and seven bands with even symmetry has strong advantages. The tight-binding model band structures can be fit to DFT band structure results with greater accuracy and simplicity, for example. Especially when the pairing interactions are introduced, this transformation reduces the speed of numerical calculations significantly and provides additional insight into physical properties of bilayer graphene.

C. Fit to DFT band structures

This formalism has been applied and divided into two separated effective single layer (shrunk)- pseudo-graphene models. DFT calculation is used to obtain the electronic structure data. Gnu-plot of DFT data has been shown with blue thin dashed lines in the background of Fig. 3(a),(b). The six odd bands and seven even bands were fit to DFT bands with results shown with color lines in the Fig. 3. The main problem that emerged here is that odd and even sector bands are not separated in the DFT data. But by inspecting the DFT band structure and to be careful in analytical calculations, knowing that odd sector does not affected by Ca-C coupling the odd and even sector flat bands can easily be distinguished. Emerging of two distinct gaps in the Dirac point of both sectors is the other guide to perform fitting. The reduced fitting parameters are given in Tables I and II.

We follow the model presented in ref. [41]. As illustrated in Fig. 1(a) on each of bilayer graphene sheets, the A_1 sublattice site of the central unit cell is chosen as the origin labeled by 0, and the B_1 site in the adjacent hexagon is considered as the second C atom neighbor. While just slightly longer than the nearest neighbor atoms B_2 and B_3 in the same hexagon, this neighbor is labeled by $n = 2$, and so on the further neighbors are labeled. In Fig. 1 (a), the big hexagon included up to nine intra-plane neighbors but for the pristine graphene it is surrounded by five neighbors. C-C hopping from 0-subsite to intra-plane n th neighbor (t_{i0jn}^{intra}) plus (minus) hopping from 0-subsite to inter-plane n th neighbor (t_{i0jn}^{inter}) has been shown by $t_{0n}^{\pm CC}$. In-plane Ca-Ca hoppings t_{0m}^{Ca-Ca} are included up to $m = 4$ neighbors. Modified Ca to C hopping integrals in Eq. 12, which are defined as $\sqrt{2}$ times the hopping from central Ca to m th neighbor C atoms, are denoted by t_{0m}^{CaC} and obtained up to $m = 5$ neighbors.

The six odd bands and seven even bands specified by Eqs. 11 and 12 respectively, have reduced hopping integrals given by $t_{im\sigma,jn\sigma}^\pm = t_{im,jn}^{inter} \pm t_{im,jn}^{intra}$, DFT calculated bands were fitted to tight binding odd bands of Eq. 15, with results presented in Fig. 3(a) and Table I. The even bands which are solutions of Eq. 12 are obtained numerically and fitted to the DFT bands. The results are illustrated in Fig. 3(b) and Table II.

There are two flat bands with d -wave Bloch character: one in each of the odd and even sectors. The opposite signs of nearest neighbor inter- and intra-layer hopping amplitudes, t_1^{11} and t_1^{12} , leads to reduced bandwidths of the even states (+ sign) in Eq. 12. Larger interlayer hopping t_1^{12} leads to smaller bandwidth ($H^\pm = H_{11} \pm H_{12}$), while for the other six odd-symmetry bands, the bandwidth can increase as can be seen in Fig. 3. On the other hand, the bandwidth of the even sector flat band is reduced, again due to the calcium to carbon hopping while the odd sector is not affected by Ca-C hoppings. For this reason, the flat band belonging to the even bands group plays a major role in superconductivity.

TABLE I: The C-C hopping parameters (in eV) for the six odd symmetry bands of C_6CaC_6 are denoted by $t_{0n}^{(-)CC}$ where the index n indicates n -th neighbour.

n	0	1	2	3	4	5	6	7	8	9
$t_{0n}^{(-)CC}$	$\epsilon_c^- = -1.00$	$t_1^- = 3.04$	$t_1'^- = 0.92t_1^-$	$t_2^- = -0.23$	$t_2'^- = 0.92t_2^-$	$t_3^- = -0.29$	$t_3'^- \approx t_3^-$	$t_4^- = -0.02$	$t_4'^- \approx t_4^-$	$t_5^- = -0.05$

TABLE II: The C-C hopping parameters (in eV) for the seven even-symmetry bands of C_6CaC_6 are denoted by $t_{0n}^{(+)\text{CC}}$ where the index n indicates the n -th neighbour. In the intercalant plane, Ca-Ca hopping parameters are denoted by t_{0m}^{CaCa} where m is m -th Ca neighbor of central Ca. The modified Ca-C hopping parameter is t_{0m}^{CaC} .

n	0	1	2	3	4	5	6	7	8	9
$t_{0n}^{(+)\text{CC}}$	$\epsilon_c^+ = -0.60$	$t_1^+ = 2.94$ $t_1'^+ = 0.92t_1$		$t_2^+ = -0.24$ $t_2'^+ = 0.92t_2$		$t_3^+ = 0.27$ $t_3'^+ \approx t_3^+$		$t_4^+ = -0.02$ $t_4'^+ \approx t_4^+$		$t_5^+ = -0.08$
m	0	1	2	3	4	5				
t_{0m}^{CaCa}	$\epsilon_{Ca} = 1.12$	-0.35	0.06	0.06	-0.02	0.00				
t_{0m}^{CaC}	-	0.17	-0.14	0.08	-0.07	-0.05				

IV. SUPERCONDUCTING PAIRING AND STATES

A. Bogoliubov-de Gennes Transformation

We treat the thirteen band Hubbard model in mean field approximation to investigate superconductivity in intercalated bilayer graphene. Singlet pairing is considered and, as illustrated in Fig. 1, pairing interactions are pictured in real space as interactions between nearest neighbors on inter- and intra-layer carbon atoms. This superconducting Hamiltonian can be transformed, as for the non-interacting case, to the direct sum of two independent superconducting Hamiltonian corresponding to odd and even symmetries pseudo-graphene structures

$$\hat{H}_{su} = \sum_{\vec{k}} \Lambda^\dagger(\vec{k}) \begin{pmatrix} H_{su}^+(\vec{k}) & 0 \\ 0 & H_{su}^-(\vec{k}) \end{pmatrix} \Lambda(\vec{k}) \quad (18)$$

where $\Lambda^\dagger(\vec{k}) = \left([\hat{c}_{0\uparrow}^\dagger(\vec{k}) \hat{c}_{1\uparrow}^\dagger(\vec{k}) \dots \hat{c}_{6\uparrow}^\dagger(\vec{k}) \hat{c}_{0\downarrow}(-\vec{k}) \hat{c}_{1\downarrow}^\dagger(-\vec{k}) \dots \hat{c}_{6\downarrow}^\dagger(-\vec{k})] \quad [\hat{c}_{1\uparrow}^\dagger(\vec{k}) \hat{c}_{2\uparrow}^\dagger(\vec{k}) \dots \hat{c}_{6\uparrow}^\dagger(\vec{k}) \hat{c}_{1\downarrow}(-\vec{k}) \hat{c}_{2\downarrow}(-\vec{k}) \dots \hat{c}_{6\downarrow}(-\vec{k})] \right)$, in which $\hat{c}_{m\sigma}^{(\pm)\dagger}(\vec{k}) = \frac{1}{\sqrt{2}}(\hat{c}_{m\sigma}^\dagger(\vec{k}) \pm \hat{c}_{m+6,\sigma}^\dagger(\vec{k}))$ and H_{su}^+ and H_{su}^- are Hamiltonians of even and odd symmetry pseudo-graphene structures respectively; for more information see Appendix C. Decoupling of these Hamiltonians means there is no effective pairing between an electron in the even sector with one in the odd sector. Using the fact that the gap is small on the electronic scale, applying perturbation up to second order gives quasiparticle energies from Eq.18 (see ref. [41]) as

$$E_{m,s}^{Q+}(\vec{k}) = s \left(E_m^+(\vec{k}) + \sum_{n=1}^7 \frac{|\Delta_{mn}^+(\vec{k})|^2}{E_m^+(\vec{k}) + E_n^+(\vec{k})} \right), \quad \Delta_{mn}^+(\vec{k}) = \sum_{\alpha=1}^9 \Omega_{mn}^{+\alpha}(\vec{k}) \Delta_+^\alpha \quad s = \pm 1, \quad m = 1, 2, \dots, 7 \quad (19)$$

$$E_{m,s}^{Q-}(\vec{k}) = s \left(E_m^-(\vec{k}) + \sum_{n=8}^{13} \frac{|\Delta_{mn}^-(\vec{k})|^2}{E_m^-(\vec{k}) + E_n^-(\vec{k})} \right), \quad \Delta_{mn}^-(\vec{k}) = \sum_{\alpha=1}^9 \Omega_{mn}^{-\alpha}(\vec{k}) \Delta_-^\alpha \quad s = \pm 1, \quad m = 8, 9, \dots, 13 \quad (20)$$

Here $(\Delta_\pm^1 \quad \Delta_\pm^2 \quad \Delta_\pm^3) = [(g_1 \Sigma_1 \pm g_1' \Sigma_1') \quad (g_1 \Sigma_2 \pm g_1' \Sigma_2') \quad (g_1 \Sigma_3 \pm g_1' \Sigma_3')]$, $(\Delta_\pm^4 \quad \Delta_\pm^5 \quad \Delta_\pm^6) = [(g_0 \Delta_1 \pm g_0' \Delta_1') \quad (g_0 \Delta_2 \pm g_0' \Delta_2') \quad (g_0 \Delta_3 \pm g_0' \Delta_3')]$ and $(\Delta_\pm^7 \quad \Delta_\pm^8 \quad \Delta_\pm^9) = [(g_0 \Pi_1 \pm g_0' \Pi_1') \quad (g_0 \Pi_2 \pm g_0' \Pi_2') \quad (g_0 \Pi_3 \pm g_0' \Pi_3')]$, where $\langle ij \rangle$ subscript has been dropped for brevity. Also

$$\begin{aligned} \Omega_{mn}^{1\pm}(\vec{k}) &= \mathcal{C}_1^*(E_m^\pm) \mathcal{C}_4(E_n^\pm) e^{i\vec{k} \cdot \vec{\tau}_1} + \mathcal{C}_4^*(E_m^\pm) \mathcal{C}_1(E_n^\pm) e^{-i\vec{k} \cdot \vec{\tau}_1} \\ \Omega_{mn}^{2\pm}(\vec{k}) &= \mathcal{C}_3^*(E_m^\pm) \mathcal{C}_6(E_n^\pm) e^{i\vec{k} \cdot \vec{\tau}_2} + \mathcal{C}_6^*(E_m^\pm) \mathcal{C}_3(E_n^\pm) e^{-i\vec{k} \cdot \vec{\tau}_2} \\ \Omega_{mn}^{3\pm}(\vec{k}) &= \mathcal{C}_2^*(E_m^\pm) \mathcal{C}_5(E_n^\pm) e^{i\vec{k} \cdot \vec{\tau}_3} + \mathcal{C}_5^*(E_m^\pm) \mathcal{C}_2(E_n^\pm) e^{-i\vec{k} \cdot \vec{\tau}_3} \\ \Omega_{mn}^{4\pm}(\vec{k}) &= \mathcal{C}_2^*(E_m^\pm) \mathcal{C}_6(E_n^\pm) e^{i\vec{k} \cdot \vec{\delta}_1} + \mathcal{C}_6^*(E_m^\pm) \mathcal{C}_2(E_n^\pm) e^{-i\vec{k} \cdot \vec{\delta}_1} \\ \Omega_{mn}^{5\pm}(\vec{k}) &= \mathcal{C}_1^*(E_m^\pm) \mathcal{C}_5(E_n^\pm) e^{i\vec{k} \cdot \vec{\delta}_2} + \mathcal{C}_5^*(E_m^\pm) \mathcal{C}_1(E_n^\pm) e^{-i\vec{k} \cdot \vec{\delta}_2} \\ \Omega_{mn}^{6\pm}(\vec{k}) &= \mathcal{C}_3^*(E_m^\pm) \mathcal{C}_4(E_n^\pm) e^{i\vec{k} \cdot \vec{\delta}_3} + \mathcal{C}_4^*(E_m^\pm) \mathcal{C}_3(E_n^\pm) e^{-i\vec{k} \cdot \vec{\delta}_3} \\ \Omega_{mn}^{7\pm}(\vec{k}) &= \mathcal{C}_3^*(E_m^\pm) \mathcal{C}_5(E_n^\pm) e^{i\vec{k} \cdot \vec{\delta}_1} + \mathcal{C}_5^*(E_m^\pm) \mathcal{C}_3(E_n^\pm) e^{-i\vec{k} \cdot \vec{\delta}_1} \end{aligned}$$

$$\begin{aligned}\Omega_{mn}^{8\pm}(\vec{k}) &= \mathcal{C}_2^*(E_m^\pm)\mathcal{C}_4(E_n^\pm)e^{i\vec{k}\cdot\vec{\delta}_2} + \mathcal{C}_4^*(E_m^\pm)\mathcal{C}_2(E_n^\pm)e^{-i\vec{k}\cdot\vec{\delta}_2} \\ \Omega_{mn}^{9\pm}(\vec{k}) &= \mathcal{C}_1^*(E_m^\pm)\mathcal{C}_6(E_n^\pm)e^{i\vec{k}\cdot\vec{\delta}_3} + \mathcal{C}_6^*(E_m^\pm)\mathcal{C}_1(E_n^\pm)e^{-i\vec{k}\cdot\vec{\delta}_3}.\end{aligned}\quad (21)$$

Here $\mathcal{C}_m(E_n^-)$ is the m th component of n th column eigenvector of H^- and $\mathcal{C}_m(E_n^+)$ is $(m+1)$ th component of n th eigenvector of $H_c^+(\vec{k})$. Band order parameters $\Delta_{mn}^+(\vec{k})$ are defined such that first electron is in the m th band and second electron is in the n th band of $H_c^+(\vec{k})$, also $\Delta_{mn}^-(\vec{k})$ is defined such that first electron is in the m th band and second electron is in the n th band of $H^-(\vec{k})$. Note that an electron in the m th band of $H_c^+(\vec{k})$ and an electron in n th band of $H^-(\vec{k})$ cannot be paired; *i.e.* for this case $\Delta_{mn}^\pm(\vec{k}) = 0$.

The Bogoliubov-de Gennes transformation used in Eq. 18 shows that pairing amplitudes should be $\Delta_\pm^\alpha = \langle \hat{c}_{\alpha,i}^\pm \hat{c}_{\alpha,j}^\pm \rangle$ which implies that all inter- and intra-layer pairing amplitudes in real space are equal, $g_0 = g'_0$ and $g_1 = g'_1$. This restriction makes the matrix gap equations hermitian and implies that band order parameters, $\Delta_{mn}^\pm(\vec{k})$ can be interpreted physically as pairing of electrons in different bands with pairing interaction g_0^\pm . In this limit $\Delta_{mn}^\pm(\vec{k})$ is equal to the product of band Green function and g_0 ,

$$\Delta_{mn}^\pm(\vec{k}) = g_0^\pm \langle \hat{d}_m^{\pm\uparrow}(\vec{k}) \hat{d}_n^{\pm\downarrow}(\vec{k}) \rangle \quad (22)$$

where $\hat{d}_i^{\pm\sigma}(\vec{k}) = \sum_{m=1}^7 \mathcal{C}_m^{\pm*}(E_i(\vec{k})) \hat{c}_m^\sigma(\vec{k})$ annihilates an electron with spin σ in the i th even or odd bands with energy $E_i^\pm(\vec{k})$.

B. Two Gap Superconducting Pairings and States

The linearized gap equation can be decoupled by minimizing free energy with respect to nearest neighbor pairing, or equivalently with respect to Δ_\pm^α , for more detail see Appendix C. Minimization of free energy with respect to Δ_\pm^α gives

$$\begin{bmatrix} A^\pm & B^\pm & B^\pm \\ B^\pm & C^\pm & D^\pm \\ B^\pm & D^\pm & C^\pm \end{bmatrix} \begin{pmatrix} \Sigma_i \pm \Sigma'_i \\ \Pi_i \pm \Pi'_i \\ \Delta_i \pm \Delta'_i \end{pmatrix} = -\frac{1}{g_0^\pm} \begin{pmatrix} \Sigma_i \pm \Sigma'_i \\ \Pi_i \pm \Pi'_i \\ \Delta_i \pm \Delta'_i \end{pmatrix} \quad (23)$$

in which A , B , C and D matrices have been introduced as

$$A^\pm = \begin{bmatrix} \Gamma_{11}^\pm & \Gamma_{12}^\pm & \Gamma_{12}^\pm \\ \Gamma_{12}^\pm & \Gamma_{11}^\pm & \Gamma_{12}^\pm \\ \Gamma_{12}^\pm & \Gamma_{12}^\pm & \Gamma_{11}^\pm \end{bmatrix}, \quad C^\pm = \begin{bmatrix} \Gamma_{44}^\pm & \Gamma_{45}^\pm & \Gamma_{45}^\pm \\ \Gamma_{45}^\pm & \Gamma_{44}^\pm & \Gamma_{45}^\pm \\ \Gamma_{45}^\pm & \Gamma_{45}^\pm & \Gamma_{44}^\pm \end{bmatrix}, \quad B^\pm = \begin{bmatrix} \Gamma_{14}^\pm & \Gamma_{15}^\pm & \Gamma_{15}^\pm \\ \Gamma_{15}^\pm & \Gamma_{14}^\pm & \Gamma_{15}^\pm \\ \Gamma_{15}^\pm & \Gamma_{15}^\pm & \Gamma_{14}^\pm \end{bmatrix}, \quad D^\pm = \begin{bmatrix} \Gamma_{47}^\pm & \Gamma_{48}^\pm & \Gamma_{48}^\pm \\ \Gamma_{48}^\pm & \Gamma_{47}^\pm & \Gamma_{48}^\pm \\ \Gamma_{48}^\pm & \Gamma_{48}^\pm & \Gamma_{47}^\pm \end{bmatrix}. \quad (24)$$

wherein, Γ matrix elements are given by

$$\Gamma_{\beta\alpha}^\pm = \frac{1}{N} \sum_{\vec{k}} \sum_i \sum_j \frac{\tanh(\frac{E_i^\pm}{2k_B T})}{E_j^\pm(\vec{k}) + E_i^\pm(\vec{k})} \left(\Omega_{ij}^{\pm\alpha}(\vec{k}) \Omega_{ji}^{\pm\beta}(\vec{k}) + \Omega_{ji}^{\pm\alpha}(\vec{k}) \Omega_{ij}^{\pm\beta}(\vec{k}) \right). \quad (25)$$

Equation 23 can be interpreted as two independent gap equations for odd (minus sign) and even (plus sign) pseudo-graphene systems. The impact is that superconductivity can be established independently in two distinct sectors this system. In the next section we numerically inspect which of these pseudo-graphene sectors, odd or even, play major roles of superconductivity.

Gholami *et al.*⁴¹ solved such gap equations for Li-decorated single layer graphene. The gap equations in Eq. 70 are the same form so they can be solved similarly. The A , B , C , and D matrices have identical structures, hence they share eigenvectors: $V_s^T = (1 \ 1 \ 1)$, $V_{d_{xy}}^T = (1 \ -1 \ 0)$, and $V_{d_{x^2-y^2}}^T = (1 \ 1 \ -2)$, where the latter two are degenerate. Their eigenvalues, in obvious notation, are

$$\begin{aligned}a_s^\pm &= \Gamma_{11}^\pm + 2\Gamma_{12}^\pm, & b_s^\pm &= \Gamma_{14}^\pm + 2\Gamma_{15}^\pm, & c_s^\pm &= \Gamma_{44}^\pm + 2\Gamma_{45}^\pm, & d_s^\pm &= \Gamma_{47}^\pm + 2\Gamma_{48}^\pm \\ a_d^\pm &= \Gamma_{11}^\pm - \Gamma_{12}^\pm, & b_d^\pm &= \Gamma_{14}^\pm - \Gamma_{15}^\pm, & c_d^\pm &= \Gamma_{44}^\pm - \Gamma_{45}^\pm, & d_d^\pm &= \Gamma_{47}^\pm - \Gamma_{48}^\pm.\end{aligned}\quad (26)$$

Similar to decorated single layer graphene⁴¹, for each of the gap equations given by Eq. 70 there are nine independent solutions. The first three superconducting states with island (localized) character can be expressed in compact form as

$$[\Psi_{\Delta_{sy}^\pm}^0]^T = [0, \quad V_{sy}, \quad -V_{sy}], \quad J_{sy}^{0\pm} = c_{sy}^\pm - d_{sy}^\pm \quad (27)$$

where V_{sy} refers to one of the V_s , $V_{d_{xy}}$ or $V_{d_{x^2-y^2}}$ -wave symmetries. Pairing in these phases cannot propagate. The other six superconducting states of Eq. 70 have the explicit form

$$[\Psi_{\Delta_{sy}^{\pm}}^l]^T = [\alpha_{sy}^{l,\pm} V_{sy}, V_{sy}, V_{sy}] \quad (28)$$

where

$$\alpha_{sy}^{l,\pm} = \frac{J_{sy}^{l,\pm} - c_{sy}^{\pm} - d_{sy}^{\pm}}{b_{sy}^{\pm}}, \quad J_{sy}^{l,\pm} = \frac{1}{2} \left(a_{sy}^{\pm} + c_{sy}^{\pm} + d_{sy}^{\pm} + (-1)^l \sqrt{8(b_{sy}^{\pm})^2 + [c_{sy}^{\pm} + d_{sy}^{\pm} - a_{sy}^{\pm}]^2} \right), \quad l = 1, 2. \quad (29)$$

Here $c_{sy} = c_s^{\pm}, c_d^{\pm}$, $b_{sy} = b_s^{\pm}, b_d^{\pm}$, $d_{sy} = d_s, d_d^{\pm}$ and $J_{sy}^{l,\pm} = -\frac{1}{g_0^{\pm}}$ for each symmetry, and + superscript refer to the even sector and - superscripts to the odd sector. In each of above categories, $d_{x^2-y^2}$ and d_{xy} phases are degenerate. Similar to decorated single layer graphene, only three of solutions for which $l = 2$ are physically reachable in the framework of mean field theory. In the limit of pristine bilayer graphene, these three states convert to usual s-wave and d-wave symmetries. In the sec. V, for odd and even sectors we illustrate from numerical solutions which of these three phases are dominant.

C. Flat band(s) Superconductivity: Strong interlayer coupling

To make a rough estimate and provide mathematical insight into the physics, one can diagonalize normal state Hamiltonian of pristine bilayer graphene in the mini-Brillouin zone of C_6CaC_6 . As shown in Fig. 3, two conduction bands corresponding to odd and even sector are weakly dispersive near the Fermi energy along $\Gamma \rightarrow M$, which seems to play a major role in the formation of superconducting Cooper's pairs.

In the case of pristine bilayer graphene, odd (-) and even (+) so called flat bands are the minimum of $(E_{\alpha,2}^{\pm}(\vec{k}), E_{\beta,2}^{\pm}(\vec{k}))$ along different high symmetry paths that are given by Eqs. 47 and 48, where their Bloch wave function, viz. Eq. 49, are similar to those of ref.⁴¹. They have linear combination of $d_{x^2-y^2}$ and d_{xy} character and are responsible for superconducting pairing $d_{x^2-y^2}$ and d_{xy} .

One can ask: what is so special about these flat bands? To address this question, we return to the matrix gap equation of Eq. 25. The right hand side contains the product of a form factor given by $\Omega_{ni}^{\alpha}(\vec{k})\Omega_{ni}^{\beta}(\vec{k}) + \Omega_{ni}^{\beta}(\vec{k})\Omega_{ni}^{\alpha}(\vec{k})$ and the thermal occupation factor over the energy denominator i.e. $\frac{\tanh(\frac{E_n}{2k_B T})}{E_n(\vec{k}) + E_i(\vec{k})}$. The form factor is a function of the Bloch wave coefficients of normal state Hamiltonian. Using Eqs. 49, 50 one can investigate that in the limited case of pristine bilayer graphene at the nearest neighbor approximation, these Bloch wave coefficients are the same for both sectors and this is almost for the next neighbor approximation. As such, it is independent of chemical potential μ . Thus the form factor is the same for the both odd and even sector of band structures. Since $\frac{\tanh(x)}{x} \rightarrow 1$ as $x \rightarrow 0$, when one of the conduction odd or even flat bands and so their corresponding valance bands becomes completely flat at the Fermi level then $\frac{\tanh(\frac{\beta E_i}{2})}{E_i(\vec{k}) + E_j(\vec{k})} \rightarrow \frac{\beta}{4}$, where $E_i(\vec{k})$ or $E_j(\vec{k})$ are one of these flat bands. In this case the dominant contribution comes from these mutual conduction and valance flat bands, and one can show that all gap equation block matrix elements in Eq. 24 are equal to A^{\pm} . In this event, depending on whether the flat bands belong to the odd or even sector, one can use Eqs. 21, 25, and 49 to show that

$$\Gamma_{11}^{\pm} \rightarrow \frac{\beta_c}{9}, \quad \Gamma_{12}^{\pm} \rightarrow -\frac{\beta_c}{36}, \quad (\beta_c = \frac{1}{k_B T_c}). \quad (30)$$

Cooper pair interaction potentials g_0 of d-wave symmetry, i.e. g_0^d and s-wave symmetry g_0^s , are given by

$$g_0^d = \frac{1}{3(\Gamma_{11}^{\pm} - \Gamma_{12}^{\pm})} = \frac{12}{5} k_B T_c$$

$$g_0^s = \frac{1}{3(\Gamma_{11}^{\pm} + 2\Gamma_{12}^{\pm})} = 6 k_B T_c \quad (31)$$

In this case $\Gamma_{12}^{\pm} < 0$ and g_0^d is less than g_0^s , so d-wave symmetry is dominant, with an extraordinary decrease in pairing potential interaction proportional to the critical temperature. This ‘‘ultra’’ decrease of pairing interaction can explain the importance of the flat bands in the formation of Cooper pairs in twisted bilayer graphene. Here, another point that can be deduced from mathematical calculations is that in the limit of strong interlayer hopping when inter-layer hoppings tends to minus (plus) of intra-layer hoppings, as one can see from Appendix D, all of the

six bands of even (odd) sector become flat while the other sector bandwidths increases. Then one can show that the gap matrix elements are

$$\Gamma_{i,j} \rightarrow \beta_c \delta_{ij}; \quad g_0 = k_B T_c \quad (32)$$

and so all possible superconducting symmetries are degenerate with pairing potential $g_0 = k_B T_c$.

V. NUMERICAL RESULTS

A. General features

To know in the variety of doping regimes which of the pairing symmetries (distorted s -wave or d -wave) are dominant, and also to inspect in the which sectors of the band structure Cooper pairs with the lowest pairing potential can constructed, superconducting gap equations of odd and even sectors *i.e.* Eq. 23 are solved numerically. The result is shown in Fig. 4.

Similar to Li intercalated single layer graphene (ref. [41]), at moderate doping, d -wave superconductivity always dominates in both sectors of the C_6CaC_6 band system. Distorted s -wave symmetry only survives at high doping levels. For odd and even sector flat bands, the density of states peaks at the M critical point. This point, for the odd flat band, is located about 0.5 eV above the Fermi level, and about 0.44 eV below the Fermi level for the case of the even flat band. Exploration of each of these flat bands can be engineered by applying a gate voltage on the bilayer via a change in the chemical potential μ . As illustrated in Fig. 4, around $\mu = 0$ at $T_c = 1K$ *i.e.* C_6CaC_6 is not affected by gate voltage. Dominant d -wave symmetry pairing phases are degenerate, so pairing can arise in both odd and even flat bands. This occurs when the averaged density of states of both bands are the same near the Fermi level. When the odd flat band is dominant near Fermi level due to electron doping, d -wave pairing dominates in this band, with the minimum of the pairing interaction energy ($g_0^- = 0.35$) corresponding to the M point near $\mu = 0.5eV$.

B. Hole doping

Hole doping by gating, by Ca \rightarrow Na substitution, or by Ca deficiency, leads to the situation where the even flat band dominates. Dominant d -wave symmetry occurs in this band with the lowest pairing energy ($g_0^+ = 0.12$), again at the critical M point at $\mu = -0.44eV$. From Fig. 4 it can be seen that when the even flat band is dominant (hole doping), the pairing potential g_0 of d -wave symmetry emerging from this band is less than the case that dominant d -wave symmetry occurs in the odd flat band (by electron doping). For example, with a factor of one-third at their critical M point *i.e.* $g_0^+ = \frac{1}{3}g_0^-$, that means that when the even flat band reaches near the Fermi level, reduction of bandwidth due to both interlayer C-C interaction (H_{12}) and C-Ca layer interactions lead to a sharp increase in the density of states. While both C-C and Ca-C interlayer interaction decrease the pairing potential g_0 , one can numerically inspect that reduction of the bandwidth due to graphene interlayer interaction, more affected the energy of pairing in the even flat band than Ca-C layers interaction.

In the case of Ca intercalated bilayer graphene, for a given T_c the pairing interaction potential g_0 (proportional to superconducting gap energy, $|\Delta|^2$) for dominant d -wave phases of the odd and even superconducting gaps are illustrated in Fig. 5. It is evident that for a given critical temperature T_c , superconductivity can be single gap or two gap and dominant superconducting pairings can occur between electrons in the odd H^- , or even H_c^+ , sector.

VI. DISCUSSION AND SUMMARY

Discovery of new superconducting phases, often at low temperature, has been one of the active achievements in recent decades. Superconductivity in the lithium-coated single layer graphene with respect to to the case of calcium-decorated single layer is more capable¹⁰ and also reported experimentally, whereas this situation is opposing in the bilayer graphene. Superconductivity has been reported in the Ca-intercalated bilayer graphene around $T_c = 4K$ while Li-intercalated bilayer graphene is not superconductor^{24,25}. Experimental fabrication of Li and Ca-intercalated bilayer graphene has been reported in the ref.²³ and ref.²² respectively. Li and Ca atoms are suggested to intercalate between graphene layers with an ordered structures similar to that of bulk GICs like LiC_6 *i.e.* two graphene layers are AA-stacking. That it demonstrates the vitally important role of intercalant inter-band in the formation of superconductivity Cooper pairs.

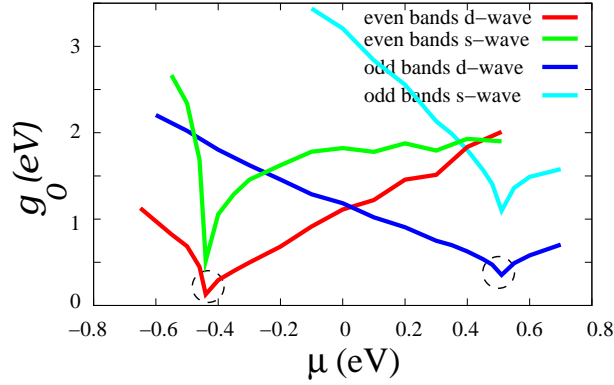


FIG. 4: Pairing interaction potential g_0 versus chemical potential μ . Both odd (six bands) and even (seven bands) symmetry solutions are shown for $T_c = 1K$. Their corresponding d -wave phases are degenerate around $\mu = 0$ and pairing separately contributes to a phase with two differing gaps. For both odd and even flat bands, d -wave symmetries are dominant at moderate doping, while at high doping a phase transition from d -wave to distorted s -wave occurs. This transition can be seen for the even flat band near $\mu = 0.5eV$. Hole doping causes the d -wave symmetry pairing to prevail between electrons in the even flat band case, with a minimum of pairing potential interaction $g_0^+ = 0.12eV$ where there occurs a critical M point at -0.44 eV shown by a dashed circle. Vice versa, electron doping leads to d -wave symmetry pairing between electrons in the odd flat band, with a minimum of pairing potential interaction at $g_0^+ = 0.12eV$ that occurs at the critical M point at -0.44 eV shown by a dashed circle.

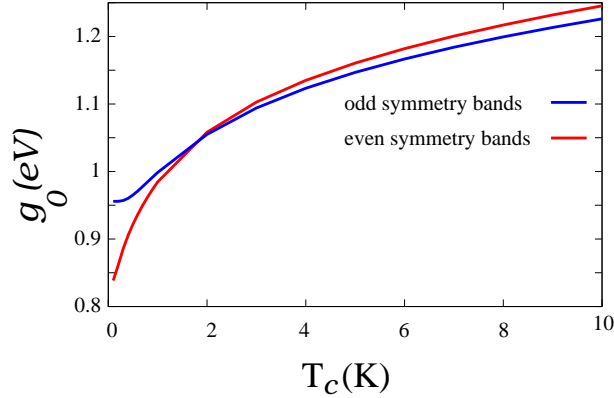


FIG. 5: Critical temperature T_c versus pairing potential g_0 . Shown are the dominant d -wave solutions of the odd (six bands) and even (seven bands) symmetry superconducting gap equations. At $T_c = 2K$ the phases are degenerate, and pairing separately contributes to a phase with two gaps.

Most theoretical microscopic models of pristine honeycomb bilayer superconductivity concentrate on the more stable AB stacking of bilayer graphene.^{27,28} To our knowledge, there are few studies that focus on pristine AA stacked bilayer graphene,³⁴ and no analogous studies that concentrate on intercalated bilayer graphene. Based on *ab initio* calculations of electron-phonon coupling, anisotropic Migdal-Eliashberg theory has been applied by some authors^{40,42} to give strong evidence that this system is a phonon mediated two-gap superconductor with predicted T_c around 7K. Recently unconventional superconductivity up to $T_c = 1.7K$ has been reported in gated twisted bilayer graphene where the layers are rotated relative to each other by a magic angle of 1.1° . Superconductivity in this low doping regime of band filling cannot be addressed within the framework of conventional electron-phonon coupling based on Migdal's adiabatic approximation. This discovery has opened speculation that this superconducting behavior may shed light on other systems in which superconductivity arises from an insulating phase.¹⁹ This development also highlights studies such as ours, which does not rely on the mechanism, but instead on more general pairing concepts and the specific electronic structure.

Many theorists have suggested that exotic superconductivity gaps arise in some materials are related to a peculiarity of the normal-state band structure. In this kind of issue angle-resolved photoemission spectroscopy (ARPES) extensively has been applied to analysis of the normal state band structure. To determine structural and electronic properties of material, tight binding model in addition to DFT calculation has been used to interpret experimental results achieved from ARPES. Following this point of view, extended Hubbard model has been used here to address

superconductivity of Ca- intercalated bilayer graphene.

The main results are achieved in two steps: first, for the normal-state (non-interacting part) a more realistic effective tight-binding model with two decoupled symmetry sectors is derived, with the parameters determined by a fitting to the DFT band structure; second, the dominant superconducting pairing channels are discussed based on a mean-field treatment of a Hubbard model obtained by adding (effective) attractive interactions between the electrons. The summary, results and comparisons are presented below.

A. Non interacting Part: Normal state

In the first part of this manuscript we have taken the advantages of mirror symmetry operation on the AA-stacked BIG through the central plane and generalized it to include intercalated bilayer graphene.

1. AA-stacked pristine bilayer graphene: Two kinds of quasiparticles

The honeycomb lattice structure makes quasi-particles in the single layer graphene behave as a massless Dirac particles at low energies that provide a proper platform to examine the characteristic effects of QED, such as the Klein paradox and Zitterbewegung, which were never observed in particle physics. In addition to relativistic nature of quasiparticles in single layer graphene, they exhibit extra aspects of such behaviors in AA-stacked BIG. Interlayer coupling causes the bilayer graphene to exhibit properties that are not observed in the single layer graphene. In QED, the 4-component "Dirac spinor" (Dirac representation) decomposes into two irreducible representations, acting only on two 2-component right and left hand "Weyl spinors." There is a pedagogically useful mathematical similarity between the Schrödinger equation of AA-BIG in these two representations and the Dirac equation. The non-interacting AA-stacked Hamiltonian is invariant under mirror symmetry, leads to division of the AA-BIG band structure into two even and odd sectors characterized by eigenvalues of mirror operation $h = \pm 1$ (analogous to two decouple Weyl equations for massless relativistic chiral particles). Each of these sectors describes a graphene-like structure i.e. H^+ and H^- . In this notion as has been shown in the Fig. 2c, up and down pseudo-spin (h-Pspin) of irreducible blocks of AA-BIG Hamiltonian viz. H^+ and H^- , consists of two electrons with the same spin which each one located at similar sub-sites in the opposing layers. These quasi-particles describe by an additional index has been called "cone index". Here we refer to this index as h-chirality index. According to this notion, one can describe Dirac cones in AA-BIG shown in the Fig. 2(b) with two kind of chirality with respect to asymmetric in such a way that the structure and its vertical ("v-chirality") and horizontal ("h-chirality") mirror image are not superimposable. This chirality (h-chirality) is a general aspect of AA-BIG quasi-particles that holds for general hoppings and over the entire Brillouin zone and it is unrelated to the helicity operation. This is in contrast to the famous graphene chirality (helicity) that occurs just at low energies near the Dirac cones.

Physically, AA-stacked BIG can be interpreted as a "single layer honeycomb lattice" that instead of $1e^-$ charge carriers, there are two types of fermionic quasi-particles with $2e^-$ charge, moving through it that differ in a quantum number called cone index (h-chirality). Quasi-particles with different h-chirality don't interact but move independently. Also (± 1) h-chiral quasi-particles have $\pm\gamma_0$ on-site energies (similar to the positive and negative energy of the particles and the anti-particles in the QED). Hopping of quasi-particles with $(+1)$ h-chirality constructs the even sector of band structure while the odd sector made by (-1) h-chiral quasiparticles. Near the Dirac cone points, quasi-particles with (± 1) h-chirality are moving with Fermi velocities v_f^\pm . One can distinguish quasi-particles with the same chirality (v-chirality) and different cone index (h-chirality) from their velocities which in the case of strong interlayer coupling could be observed experimentally.

2. Intercalated AA-staked bilayer graphene: Mirror symmetry operation advantage

Based on mean-field treatment of an extended Hubbard model, a realistic thirteen band tight binding model, has been constructed to include the case of experimentally observed structures such as Ca intercalated bilayer graphene, where its parameters are determined by a fitting to DFT band structure. We followed the notion that Calcium doped bilayer graphene as the thinnest limit of graphite intercalation compounds (Fig.1(a)).

In our previous work, the effects of Li-decoration on structural and electronic band structure of single layer graphene has been demonstrated in details and also symmetry character of the band-branches illustrated as well as the possible superconducting phases of lithium decorated single layer graphene LiC_6 were obtained analytically and analyzed.⁴¹ The Brillouin zone (BZ) of these structure is one third of that of graphene, with the Dirac points folded back to the Γ point. In this mini-BZ, the two π bands of (pristine) graphene folds to six branches and their different symmetries

(d+id, s,...) are also separated as illustrated in Fig. 2 of ref. [41]. Generalization of these results to include intercalated bilayer graphene (IBIG) has strong advantages and provides additional insight into its physical properties. This is possible through decoupling of normal and superconducting Hamiltonians of IBIG into two independent corresponding single layer pseudo-graphene Hamiltonians, coupled only by a common chemical potential.

Similar to the pristine AA-staked BIG, accounting for symmetries of Bloch wave coefficients, the 13×13 Hamiltonian of IBIG converts, by mirror symmetry, to two decouple sectors: an 7×7 even symmetry sector H_c^+ with involvement of the intercalant (coated single layer pseudo-graphene) and the 6×6 odd sector H^- , for which the intercalant provides only renormalized hopping amplitudes and break down symmetry of hopping integrals (six bands shrunken single layer pseudo-graphene). Therefore, all previous discussions about $2e^-$ charge, h-Pspin and chirality of quasiparticles in pristine AA-stacked BIG are extended to include IBIG.

Periodic perturbation of graphene layers potential due to ordered Intercalant atoms causes hopping integrals symmetry to break and so two distinct gaps of size $E_g^\pm = 2|t_{11}^\pm - t'_{11}^\pm|$ open at the Dirac point (folded to Γ point) of each of the even and odd sector pseudo-graphene structures. These two gaps are characteristic of AA-IBIG. Knowing the size of these energy gaps, one can find the difference in the first nearest neighbor intra and inter-layer hopping parameters symmetry breaking i.e. $(\Delta t = t_{11} - t'_{11})$ and $(\Delta \gamma = t_{12} - t'_{12})$. In the case of Li- intercalated BIG, experimental ARPES spectra (Fig. 4 Ref.²³) shows two distinct gaps of wide $E_g^- = 0.20eV$ and $E_g^+ = 0.46eV$. We slightly correct the discussion that has been stated in the [Sec. III, sub-sec.C of Ref.²³] about the relation between these two gaps and symmetry breaking interlayer coupling parameters.

In the case of Li- intercalated BIG, Li-s orbital is fully ionized and Li-C hybridization is negligible, so the odd and even sector band structure are similar to the band structure of pristine shrunken-graphene C_6 . The difference of course is due to \pm sign that appears in the even and odd sectors between intra and inter layer hopping terms which leads to different bandwidth. The even and odd sectors Schrödinger equation solved analytically (or nearly so). From the beginning, the Hamiltonian is generalized to incorporate several broken symmetries, including the on-site energies, hopping integrals, and bonds lengths (geometry). Due to this generalization, it can be used to obtain analytic dispersion energies of not only C_6CaC_6 , but also related graphene-like structures such as $B_3N_3CaB_3N_3$.

3. Tight Binding Parametrization of Ca- intercalated bilayer graphene from DFT

Dividing the thirteen bands into seven even-symmetry bands and six odd-symmetry bands, considerably facilitates tight Binding Parametrization from DFT. We used up to nine neighbor approximation tight binding model considering the symmetry breaking of bond length and hopping integral parameters across different direction of hexagons. The main problem with DFT data is that the odd and even sector data bands are not separated. But by inspecting the DFT band structure and to be careful in analytical calculations (knowing that odd sector does not affected by Ca-C coupling directly and so remain graphen like), the odd and even sector DFT flat bands can easily be distinguished. Emerging of two distinct gaps in the Dirac point of both sectors is the other guide to perform fitting. The reduced fitting parameters are given in Tables I and II with results are shown in the Fig. 3.

B. Interacting Part: Superconductivity

SA show that electron transport across a barrier must conserve the cone index, a consequence of the Klein tunneling behavior in AA-stacked BIG. Here it is discussed that Cone index footprint can be traced also in the formation of superconducting Cooper pairs. Due to this index, the salient differences are emerged between the Cooper pairs in single layer graphene and AA-stacked bilayer graphene. The two types of even and odd symmetry superconductivity are predictable in AA-stacked bilayer graphene.

1. Odd/ Even Superconducting Gap equations and Symmetry Phases

Similar to the normal state Hamiltonian, the superconducting Hamiltonian is also block diagonalized into two sectors. Each of these two blocks represents the superconducting Hamiltonian of the even and odd single layer pseudo-graphene structures. The impact is that superconductivity in AA-stacked BIG can be established independently in two distinct band structure sectors. Two quasi particles (i.e. “four electrons”) just with the same h-chirality (i.e. cone index) can team up to build a Cooper pair (Fig. 2c). In the other words, pairing in bilayer graphene arises between quasiparticles inside of the coated single layer pseudo-graphene H_c^+ band structure (even sector-superconductivity) or uncoated shrunken single layer pseudo-graphene H^- (odd sector-superconductivity) separately; even-odd pairing is impossible without further symmetry breaking.

Two distinct superconductivity gap equations corresponding to H_c^+ and H^- single layer pseudo-graphene structures emerged from minimization of the free energy. These behaviors show that general aspects of superconductivity in the (Li-)decorated single layer graphene⁴¹ and (Ca-) intercalated bilayer graphene are similar, and their behaviors are different primarily in the probability of two gap superconductivity in the bilayer structures. A difference of course is that interlayer interaction becomes a key factor; the Cooper pairs in AA-stacked BIG instead of $2e^-$ charge have $4e^-$ charge and additionally have an right or left hand h-chirality index. This theoretical prediction requires empirical inspect.

These two even and odd superconducting gap equations were solved analytically to obtain the relations between the superconducting pairing potential and resulting ordered phases. The two sets of gap equations have solutions similar to those obtained in our previous work, for decorated single layer graphene.⁴¹ Seven hybridized orbitals in pseudo-coated single layer graphene support nine possible bond pairing amplitudes. There are nine superconducting phases with $p_x, p_y, f, s^\pm, d_{xy}^\pm$ and $d_{x^2-y^2}^\pm$ atomic orbital-like symmetries corresponding to each of these even(+)/odd(-) gap equations. Only three of them are physically reachable, denoted by $\Psi_{2,s}^\pm, \Psi_{2,dxy}^\pm$, and $\Psi_{2,d_{x^2-y^2}}^\pm$. These symmetries almost preserve properties from a two band model of pristine graphene (Fig. 4 Ref.⁴¹). The d -wave solutions are degenerate and so it can support chiral $d_{x^2-y^2} + id_{xy}$ superconductivity in each of these sectors. These three phases are distorted by intercalation. In fact, the significant difference which appears between two bands pristine C_2 pairing symmetries and shrunken graphene C_6 (decorated graphene) is a skewness factor i.e. $\alpha_{sy}^{l,\pm} \neq 1$ in front of the self consistent gaps solutions. In each of these even or odd sectors, one band is weakly dispersive near the Fermi energy along $\Gamma \rightarrow M$ where its Bloch wave function has linear combination of $d_{x^2-y^2}$ and d_{xy} character, and is responsible for $d_{x^2-y^2}$ and d_{xy} pairing with lowest pairing energy in our model(see Ref.⁴¹). Because of the high density of states of carriers in this band, d-wave superconductivity is more robust against disorder than s-wave.

2. Dominant Bands: Possibility of Two Gap superconductivity

Superconductivity could be established in the odd or even sector of intercalated AA-stacked or simultaneously in both sectors. Even/odd sectors are coupled just via chemical potential. Two nearly ‘‘flat bands’’ with d-wave symmetry Bloch character, crossing the Fermi energy, each related to the graphene-like structures, are responsible for two distinct d-wave superconductivity gaps that could be emerged. The distorted s-wave superconductivity is constructed between quasi-particles in upper bands of both sector that have s-wave symmetry character. At moderate doping, distorted d-wave superconductivity is dominant in both sectors while in high doping, distorted s-wave becomes preferable. Superconductivity with different phases in each of these sectors e.g. distorted s-wave in one sector and d-wave phase symmetry in the other, is not so possible.

To know whether superconductivity in IBIG is single gap or multi gap, depending on what type of intercalant is used, one can inspect numerically which sector will prevail. Hybridization of Carbon (CP_z) and intercalant (I_s) orbitals, electron or hole doping factor (chemical potential), nearest neighbor hopping symmetry breaking (Γ gap opening) and interlayer coupling (H_{12}) are important factors in specifying superconductivity pairing symmetry and dominant bands. While just the even sector is under the influence of C-I orbital hybridization and odd sector bands does not affected directly (except an small gap opening), but interlayer coupling has a dual effects. It reduces the bandwidth of one sector (e.g. the even sector) but simultaneously it increases the bandwidth of the other sector(e.g. odd sector). It therefore plays a crucial role in electronic correlation effects.

Mathematical analysis shows that in the limit of strong interlayer hopping, so that inter- and intra- layer hoppings are the same (up to a minus sign), then bandwidths of the odd (even) sector become completely flat while the bandwidths of the other sector are doubled. In this case superconductivity established in the flat band sector, even with a small Cooper pairing potential g_0 , leads to a high critical temperature *i.e.* $k_B T_c = g_0$. In this limit all of the possible superconducting phases, *i.e.* d, p and s -wave symmetries, are degenerate. This observation suggests there may be some aspect of unconventional superconductivity in bilayer AA- graphene related to inter- versus intralayer hopping effects be available under high pressure.

The best conditions to induced superconductivity in IBIG are those that interlayer coupling be strong and band structure of even or odd sector or both slightly be deviated from pristine graphen-like structures. Under these circumstances if electron or hole doping causes the nearly flat bands of odd or even sector meet the Fermi surface then chiral $d + id$ odd or even superconductivity may induce. An inadequate inspecting of the band structure of different metal intercalated C_6MC_6 (M=Li, Na, K, Rb, Cs, Gr, Be, Mg, Ca, Sr and Ba) such as that can be seen in the Fig. 3(a) of Ref.⁴³, shows that odd sector flat band (not affected by I-C orbital coupling) always lay on top of even sector flat band, that means the interlayer coupling t_{12} in all of them is positive. The structures in which interlayer (IL) band is empty have negligible I-C coupling and so both even and odd sector have the structure similar to shrunken graphene C_6 . The even band of Li intercalated BIG meet the Fermi Surface and interlayer coupling is stronger than the others.

These is an interesting structure that could host even-superconducting beside normal odd-Dirac quasi-particles. But since IL band is empty, symmetry not allow out of plane phonon vibration to trigger superconductivity. However it may exhibit richer correlation effect than single layer graphene under pressure, gating or proximity effects. K and Rb intercalated BIG have potential to exhibit superconductivity, while in Gr intercalated BIG it seems that simultaneous odd and even Dirac cones coexist.

Experimental evidence for superconductivity in Ca- intercalated BIG has been reported. Motivated by this observation we performed numerical calculation for C_6CaC_6 . Numerical calculations show that for both even and odd sector gap equations, d -wave phases, *i.e.* $\Psi_{\pm, d_{xy}}^2$ and $\Psi_{\pm, d_{x^2-y^2}}^2$, are dominant (smaller g_0 means less interaction energy for pairing) and slightly distorted by intercalation *i.e.* $\alpha_d^{2,\pm} \approx 1$ while s -wave symmetry *i.e.* $\Psi_{\pm, s}^2$ require greater energy and are significantly distorted, $\alpha_s^{2,\pm} \neq 1$. Phase Transition from d -wave single-gap to d -wave dual-gap Superconductivity in calcium intercalated bilayer graphene is possible. Although T_c experimentally around 4K and theoretically calculated near 6K are reported, also using Raman spectroscopy, possibility of distinguishing intralayer and interlayer electron-phonon interactions in samples of twisted bilayer graphene has been reported by ref.[35] relying on these results, from Fig. 5 it can be seen that both even and odd d -wave phases are nearly degenerate at 2K, consistent with this system being a two gap superconductor around $T_c \approx 2K$. Our results support two d -wave gap superconductivity that has been proposed in ref.[40] (Fig. 2), although different sectors were not separated in their studies.

Relying on pre-mentioned properties, AA-stacked bilayer graphene may exhibit feature-rich electronic properties than singlelayer graphen. It seems that study of superconductivity in pristine and intercalated AA-stacking BIG could tend to interesting experimental achievements- such as (even and odd) chiral superconducting $d + id$ pairing which has been predicted primarily in pristine single layer graphene at van Hove singularity point, and also simultaneous coexistence of different phases *e.g.* superconductivity and normal Dirac quasiparticles or two gap superconductivity (with different chirality) in different branches of their band-structures.

VII. ACKNOWLEDGMENTS

R. Gholami acknowledges support that allowed an extended visit to the University of California Davis during part of this work. W.E.P. was supported by NSF grant DMR-1207622.

VIII. REFERENCES

-
- * Electronic address: rmoradian@razi.ac.ir
- ¹ C. Brun, T. Cren, and D. Roditchev, Review of 2D superconductivity: the ultimate case of epitaxial monolayers, *Supercond. Sci. & Technol.* **30**, 013003 (2017).
 - ² Y. Saito, T. Nojima & Y. Iwasa Highly crystalline 2D superconductors *Nature Reviews Materials* 2, 16094 (2016).
 - ³ Nandkishore, R., Levitov, L. S. & Chubukov, A. V. Chiral superconductivity from repulsive interactions in doped graphene. *Nat. Phys.* 8, 158163 (2012).
 - ⁴ Nandkishore, R., Thomale, R. & Chubukov, A. V. Superconductivity from weak repulsions in hexagonal lattice systems. *Phys. Rev. B* 89, 144501 (2014).
 - ⁵ Black-Schaffer, A. M. & Doniach, S. Resonating valence bonds and mean field d -wave superconductivity in graphene. *Phys. Rev. B* 75, 134512 (2007).
 - ⁶ Uchoa, B. & Castro Neto, A. Superconducting States of Pure and Doped Graphene. *Phy. Rev. Lett.* 98, 146801 (2007)
 - ⁷ Kiesel, M. L., Platt, C., Hanke, W., Abanin, D. A. & Thomale, R. Competing many-body instabilities and unconventional superconductivity in graphene. *Phys. Rev. B* 86, 020507R (2012).
 - ⁸ Ma, T., Yang, F., Yao, H. & Lin, H. Q. Possible triplet $p + ip$ superconductivity in graphene at low filling. *Phys. Rev. B* 90, 245114 (2014).
 - ⁹ G. Profeta, M. Calandra, and F. Mauri, Phonon-mediated super- conductivity in graphene by lithium deposition, *Nat. Phys.* 8, 131 (2012).
 - ¹⁰ B.M. Ludbrook *et al.*, Evidence for superconductivity in Li-decorated monolayer graphene, *Proc. Natl. Acad. Sci. (USA)* **112**, 11795-11799 (2015).
 - ¹¹ T. E. Weller *et al.*, Superconductivity in the intercalated graphite compounds C_6Yb and C_6Ca , *Nat. Phys.* **1**, 39 (2005).
 - ¹² A. P. Tiwari, S. Shin, D. Hwang, S. G. Jung, T. Park, and H. Lee, Superconductivity at 7.4K in few layer graphene by Li intercalation, *J. Phys.: Condens. Matt.* **29**, 445701 (2017).
 - ¹³ Xue, M., Chen, G., Yang, H. & Zhu, Y. Superconductivity in potassium-doped few-layer graphene. *J. Am. Chem. Soc.* 134,65366539 (2012).

- ¹⁴ AV Rozhkov, AO Sboychakov, AL Rakhmanov, F Nori, Electronic properties of graphene-based bilayer systems, *Physics Reports* 648, 1-104 (2016)
- ¹⁵ Z. Liu, K. Suenaga, P. J. F. Harris, and S. Iijima, Open and Closed Edges of Graphene Layers, *Phys. Rev. Lett.* 102, 015501 (2009).
- ¹⁶ J. Borysiuk, J. Soltys, and J. Piechota, Stacking sequence dependence of graphene layers on SiC (0001) Experimental and theoretical investigation, *J. Appl. Phys.* 109, 093523 (2011)
- ¹⁷ J.-K. Lee, S.-Ch. Lee, J.-P. Ahn, S.-Ch. Kim, J. I. B. Wilson, and P. John, The growth of AA graphite on (111) diamond, *J. Chem. Phys.* 129, 234709 (2008)
- ¹⁸ Cao, Y. et al. Correlated insulator behaviour at half-filling in magic-angle graphene superlattices. *Nature* 556, <https://doi.org/10.1038/nature26154> (2018)
- ¹⁹ Y. Cao, V Fatemi, S. Fang, K. Watanabe, T. Taniguchi, E. Kaxiras, and P. Jarillo-Herrero, Unconventional superconductivity in magic-angle graphene superlattices, *Nature* **556**, 43 (2018). doi:10.1038/nature26160.
- ²⁰ MacDonald A. H., Trend: Bilayer Graphenes Wicked, Twisted Road, *Physics* **12** 12 (2019)
- ²¹ G. Chen et al., Signatures of gate-tunable superconductivity in trilayer graphene/boron nitride moiré superlattices, *Nature* 572, 215-219 (2019)
- ²² Kanetani, K.; Sugawara, K.; Sato, T.; Shimizu, R.; Iwaya, K.; Hitosugi, T.; Takahashi, T. Ca Intercalated Bilayer Graphene as A Thinnest Limit of Superconducting C6Ca. *Proc. Natl. Acad. Sci. U. S. A.* 2012,109, 19610
- ²³ Caffrey, N.M.; Johansson, L.I.; Xia, C.; Armiento, R.; Abrikosov, I.A.; Jacobi, C. Structural and electronic properties of Li-intercalated graphene on SiC(0001). *Phys. Rev. B* 2016, 93, 195421.
- ²⁴ S. Ichinokura *et al.*, Superconducting calcium-intercalated bilayer graphene, *ACS Nano* **10**, 2761 (2016).
- ²⁵ J. Chapman *et al.*, Superconductivity in Ca-doped graphene laminates, *Sci. Rep.* **6**, 23254 (2016).
- ²⁶ J. Velasco Jr., L. Jing, W. Bao, Y. Lee, P. Kratz, V. Aji, M. Bockrath, C. Lau, C. Varma, R. Stillwell, et al., Transport spectroscopy of symmetry-broken insulating states in bilayer graphene, *Nat. Nanotechnol.* 7 (2012) 156.
- ²⁷ J. Vucicevic, M. O. Goerbig, and M. V. Milovanovic, *d*-wave superconductivity on the honeycomb bilayer, *Phys. Rev. B* **86**, 214505 (2012).
- ²⁸ J. M. Murray and O. Vafek, Excitonic and superconducting orders from repulsive interaction on the doped honeycomb bilayer, *Phys. Rev. B* **89**, 205119 (2014)
- ²⁹ Hosseini, M. V. & Zareyan, M. Model of an exotic chiral superconducting phase in a graphene bilayer. *Phys. Rev. Lett.* 108, 147001 (2012).
- ³⁰ A.L. Rakhmanov, A.V. Rozhkov, A.O. Sboychakov, F. Nori, Instabilities of the AA-stacked graphene bilayer, *Phys. Rev. Lett.* 109 (2012) 206801.
- ³¹ R.S. Akzyanov, A.O. Sboychakov, A.V. Rozhkov, A.L. Rakhmanov, F. Nori, AA-stacked bilayer graphene in an applied electric field: Tunable antiferromagnetism and coexisting exciton order parameter, *Phys. Rev. B* 90 (2014) 155415.
- ³² A.O. Sboychakov, A.V. Rozhkov, A.L. Rakhmanov, F. Nori, Antiferromagnetic states and phase separation in doped AA-stacked graphene bilayers, *Phys. Rev. B* 88 (2013) 045409
- ³³ A.O. Sboychakov, A.L. Rakhmanov, A.V. Rozhkov, F. Nori, Metal-insulator transition and phase separation in doped AA-stacked graphene bilayer, *Phys. Rev. B* 87 (2013) 121401.
- ³⁴ M. Alidoust, M. Willatzen & A. Jauho, Symmetry of superconducting correlations in displaced bilayers of graphene, *Phys. Rev. B* 99, 155413 (2019)
- ³⁵ G. S. N. Eliel & et al. Intralayer and interlayer electron-phonon interactions in twisted graphene heterostructures, *Nat. Comm.* 9, 1221 (2018).
- ³⁶ S. Fang *et al*, Electric field-induced chiral *d + id* superconducting state in AA-stacked bilayer graphene: A quantum Monte Carlo study, arXiv:1907.10236
- ³⁷ Y. Endo *et al*, Structure of Superconducting Ca-intercalated Bilayer Graphene/SiC studied using Total-Reflection High-Energy Positron Diffraction, arXiv:1906.11535
- ³⁸ M. Sanderson, Y.S. Ang, C. Zhang, Klein tunneling and cone transport in AA-stacked bilayer graphene, *Phys. Rev. B* 88 (2013) 245404.
- ³⁹ M. Putti *et al*, Observation of the crossover from two-gap to single-gap superconductivity through specific heat measurements in neutron-irradiated MgB2. *Phys. Rev. Lett.* 96, 077003 (2006)
- ⁴⁰ E. R. Margine, H. Lambert, and F. Giustino, Electron-phonon interaction and pairing mechanism in superconducting Ca-intercalated bilayer graphene, *Sci. Rep.* **6**, 21414 (2016).
- ⁴¹ R. Gholami, R. Moradian, S. Moradian, W. E. Pickett, Superconducting phases of lithium intercalated graphene, *Sci. Rep.* **8**, 13795 (2018). doi: 10.1038/s41598-018-32050-9.
- ⁴² Durajski, A.; Skoczylas, K.; Szczesniak, R. Superconductivity in bilayer graphene intercalated with alkali and alkaline earth metals. *Phys. Chem. Chem. Phys.* 2019, 21, 5925.
- ⁴³ T. Kaneko and R. Saito, First-Principles Study on Interlayer State in Alkali and Alkaline Earth Metal Atoms Intercalated Bilayer Graphene, *Surface Science*, vol. 665, 19, (2017).

IX. AUTHOR CONTRIBUTIONS

R.G. and R.M. conceived of the presented idea. R.G. developed the theory and performed the computations. R.M. and W. E. P verified the analytical methods. R.M. supervised the project. R.G, R. M. and W. E. P. discussed the

results and commented on the manuscript. S. M performed DFT calculation and designed the figures.

X. ADDITIONAL INFORMATION

Competing interests: The authors declare no competing interests.

XI. APPENDIX A: ACCURATE TIGHT BINDING MODEL

In our previous work we used realistic multiband tight binding model for decorated monolayer graphene and obtained its band structure analytically.⁴¹ Here we follow and generalize that method and find analytic solutions for the intercalated bilayer graphene spectrum in general form. We consider Bloch ket state of Eq.8 as

$$|\Psi_{\vec{k}}(\vec{r})\rangle = \frac{1}{\sqrt{N}} \sum_{n=1}^N \sum_{\alpha=0}^{12} \mathcal{C}_{\alpha} e^{i\vec{k}\cdot\vec{r}_{n\alpha}} |\phi_{n\alpha}\rangle \quad (33)$$

in which $\vec{r}_{n\alpha} = \vec{r}_n + \vec{d}_{\alpha}$ and \vec{r}_n is n th Bravais lattice site vector position and \vec{d}_{α} is vector position of the α -th subsite with respect to unit cell n . The Ca sublattice is labeled by $\alpha = 0$ also $A_1^1, A_2^1, A_3^1, B_1^1, B_2^1, B_3^1, A_1^2, A_2^2, A_3^2, B_1^2, B_2^2, B_3^2$ subsites are labeled by $\alpha = 1, \dots, 12$ respectively. $|\phi_{n\alpha}\rangle = |\phi_{n\alpha}(\vec{r} - \vec{r}_n - \vec{d}_{\alpha})\rangle$ is the atomic π electron ket state of subsite α of site n . The Schrödinger equation for this system is

$$\sum_{\beta=0}^{12} \varepsilon_{\alpha\beta}(\vec{k}) \mathcal{C}_{\beta} + (\varepsilon_{\alpha} - \mu_o) \mathcal{C}_{\alpha} = E(\vec{k}) \mathcal{C}_{\alpha} \quad \text{where} \quad \varepsilon_{\alpha\beta}(\vec{k}) = -\frac{1}{N} \sum_{ij} e^{i\vec{k}\cdot(\vec{r}_{i\alpha} - \vec{r}_{j\beta})} t_{i\alpha j\beta}^{\sigma\sigma}. \quad (34)$$

Symmetries of this system imply that $\mathcal{C}_{\alpha}(\vec{k}) = \pm \mathcal{C}_{\alpha+6}(\vec{k})$. The Schrödinger equation Eq.34 can be written in the following 13×13 matrix form eigenvalue problem

$$H_N(\vec{k}) \Psi_N(\vec{k}) = \begin{bmatrix} h_0(\vec{k}) & | & h_{01}(\vec{k}) & h_{02}(\vec{k}) \\ \hline h_{10}(\vec{k}) & | & H_{11}(\vec{k}) & H_{12}(\vec{k}) \\ \hline h_{20}(\vec{k}) & | & H_{21}(\vec{k}) & H_{22}(\vec{k}) \end{bmatrix} \begin{pmatrix} \mathcal{C}_0(\vec{k}) \\ \mathbf{C}(\vec{k}) \\ \pm \mathbf{C}(\vec{k}) \end{pmatrix} = E_{\pm}(\vec{k}) \begin{pmatrix} \mathcal{C}_0(\vec{k}) \\ \mathbf{C}(\vec{k}) \\ \pm \mathbf{C}(\vec{k}) \end{pmatrix} \quad (35)$$

where the column matrix $\mathbf{C}(\vec{k})$ is $\mathbf{C}(\vec{k}) = (\mathcal{C}_1(\vec{k}) \mathcal{C}_2(\vec{k}) \dots \mathcal{C}_6(\vec{k}))^T$ and the dispersion matrices satisfy $H_{11} = H_{22}$, $H_{12} = H_{21}$ and $h_{01} = h_{02} = h_{10}^{\dagger} = h_{20}^{\dagger}$. The Ca-C dispersion row matrices $h_{01}(\vec{k}) = h_{02}(\vec{k}) = (h_{CaA}(\vec{k}) \ h_{CaB}(\vec{k}))$ are given by

$$\begin{aligned} h_{CaA}(\vec{k}) &= (\varepsilon_{CaA_1}(\vec{k}) \ \varepsilon_{CaA_2}(\vec{k}) \ \varepsilon_{CaA_3}(\vec{k})) = -t_1^{CaC} \begin{pmatrix} e^{i\vec{k}\cdot\vec{\delta}_1} & e^{i\vec{k}\cdot\vec{\delta}_3} & e^{i\vec{k}\cdot\vec{\delta}_2} \end{pmatrix} \\ h_{CaB}(\vec{k}) &= (\varepsilon_{CaB_1}(\vec{k}) \ \varepsilon_{CaB_2}(\vec{k}) \ \varepsilon_{CaB_3}(\vec{k})) = -t_1^{CaC} \begin{pmatrix} e^{-i\vec{k}\cdot\vec{\delta}_1} & e^{-i\vec{k}\cdot\vec{\delta}_3} & e^{-i\vec{k}\cdot\vec{\delta}_2} \end{pmatrix}. \end{aligned} \quad (36)$$

Here t_i^{CaC} is the hopping amplitude from Ca to i th neighbor C atom. The Ca-Ca dispersion is $h_0(\vec{k}) = \varepsilon_{CaCa}(\vec{k}) + \varepsilon_{Ca} - \mu_o$ where

$$\begin{aligned} \varepsilon_{CaCa}(\vec{k}) &= 2t_1^{CaCa} \left(\cos \vec{k}\cdot\vec{\xi}_1 + \cos \vec{k}\cdot\vec{\xi}_2 + \cos \vec{k}\cdot\vec{\xi}_3 \right) + 2t_2^{CaCa} \left(\cos \vec{k}\cdot(\vec{\xi}_1 - \vec{\xi}_2) + \cos \vec{k}\cdot(\vec{\xi}_1 - \vec{\xi}_3) + \cos \vec{k}\cdot(\vec{\xi}_2 - \vec{\xi}_3) \right) \\ &+ 2t_3^{CaCa} \left(\cos 2\vec{k}\cdot\vec{\xi}_1 + \cos 2\vec{k}\cdot\vec{\xi}_2 + \cos 2\vec{k}\cdot\vec{\xi}_3 \right) + \dots \end{aligned} \quad (37)$$

The interlayer dispersion matrices H_{11} , H_{22} and interlayer dispersion matrices H_{12} and H_{21} are given by

$$H_{mn}(\vec{k}) = \begin{pmatrix} h_{AA}^{mn}(\vec{k}) + (\varepsilon_A^m - \mu_0) \delta_{mn} I_{3 \times 3} & h_{AB}^{mn}(\vec{k}) \\ h_{BA}^{mn}(\vec{k}) & h_{BB}^{mn}(\vec{k}) + (\varepsilon_B^m - \mu_0) \delta_{mn} I_{3 \times 3} \end{pmatrix} \quad (38)$$

where the off-diagonal carbon-carbon dispersion matrices are

$$h_{AA}^{mn}(\vec{k}) = h_{BB}^{*mn}(\vec{k}) = \begin{pmatrix} \varepsilon_{A_1^m A_1^n}(\vec{k}) & \varepsilon_{A_1^m A_2^n}(\vec{k}) & \varepsilon_{A_1^m A_3^n}(\vec{k}) \\ \varepsilon_{A_2^m A_1^n}(\vec{k}) & \varepsilon_{A_2^m A_2^n}(\vec{k}) & \varepsilon_{A_2^m A_3^n}(\vec{k}) \\ \varepsilon_{A_3^m A_1^n}(\vec{k}) & \varepsilon_{A_3^m A_2^n}(\vec{k}) & \varepsilon_{A_3^m A_3^n}(\vec{k}) \end{pmatrix} = \begin{pmatrix} \alpha^{mn}(\vec{k}) & \beta^{mn}(\vec{k}) & \gamma^{mn}(\vec{k}) \\ \beta^{*mn}(\vec{k}) & \alpha^{mn}(\vec{k}) & \theta^{mn}(\vec{k}) \\ \gamma^{*mn}(\vec{k}) & \theta^{*mn}(\vec{k}) & \alpha^{mn}(\vec{k}) \end{pmatrix} \quad (39)$$

$$h_{AB}^{mn}(\vec{k}) = h_{BA}^{\dagger mn}(\vec{k}) = \begin{pmatrix} \varepsilon_{A_1^m B_1^n}(\vec{k}) & \varepsilon_{A_1^m B_2^n}(\vec{k}) & \varepsilon_{A_1^m B_3^n}(\vec{k}) \\ \varepsilon_{A_2^m B_1^n}(\vec{k}) & \varepsilon_{A_2^m B_2^n}(\vec{k}) & \varepsilon_{A_2^m B_3^n}(\vec{k}) \\ \varepsilon_{A_3^m B_1^n}(\vec{k}) & \varepsilon_{A_3^m B_2^n}(\vec{k}) & \varepsilon_{A_3^m B_3^n}(\vec{k}) \end{pmatrix} = \begin{pmatrix} \tau_1^{mn}(\vec{k}) & d_2^{mn}(\vec{k}) & d_3^{mn}(\vec{k}) \\ d_2^{mn}(\vec{k}) & \tau_3^{mn}(\vec{k}) & d_1^{mn}(\vec{k}) \\ d_3^{mn}(\vec{k}) & d_1^{mn}(\vec{k}) & \tau_1^{mn}(\vec{k}) \end{pmatrix} \quad (40)$$

in which m and n are layer index. Shorthand notation has been introduced as follows:

$$\begin{aligned} \beta^{mn}(\vec{k}) &= \varepsilon_{A_1^m A_2^n}(\vec{k}) = \varepsilon_{A_2^m A_1^n}^*(\vec{k}) = t_2^{mn} e^{i\vec{k} \cdot (\vec{\delta}_3 - \vec{\delta}_1)} \left[1 + w_t \left(e^{-i\vec{k} \cdot \vec{\xi}_3} + e^{i\vec{k} \cdot \vec{\xi}_1} \right) \right] \\ \gamma^{mn}(\vec{k}) &= \varepsilon_{A_1^m A_3^n}(\vec{k}) = \varepsilon_{A_3^m A_1^n}^*(\vec{k}) = t_2^{mn} e^{i\vec{k} \cdot (\vec{\delta}_2 - \vec{\delta}_1)} \left[1 + w_t \left(e^{-i\vec{k} \cdot \vec{\xi}_2} + e^{i\vec{k} \cdot \vec{\xi}_1} \right) \right] \\ \theta^{mn}(\vec{k}) &= \varepsilon_{A_2^m A_3^n}(\vec{k}) = \varepsilon_{A_3^m A_2^n}^*(\vec{k}) = t_2^{mn} e^{i\vec{k} \cdot (\vec{\delta}_2 - \vec{\delta}_3)} \left[1 + w_t \left(e^{-i\vec{k} \cdot \vec{\xi}_2} + e^{i\vec{k} \cdot \vec{\xi}_3} \right) \right] \\ \alpha^{mn}(\vec{k}) &= \varepsilon_{A_i^m A_i^n}(\vec{k}) = \varepsilon_{B_i^m B_i^n}(\vec{k}) = t_0^{mn} + 2t_5^{mn} \left(\cos \vec{k} \cdot \vec{\xi}_1 + \cos \vec{k} \cdot \vec{\xi}_2 + \cos \vec{k} \cdot \vec{\xi}_3 \right) \end{aligned} \quad (41)$$

and it has been supposed that $w_t = \frac{t_1^{\prime mn}}{t_1^{mn}} = \frac{t_2^{\prime mn}}{t_2^{mn}} = \dots$ and $\vec{\xi}_i = \vec{\tau}_i + 2\vec{\delta}_i$. The τ and d -functions are given by

$$\begin{aligned} \tau_1^{mn}(\vec{k}) &= e^{i\vec{k} \cdot \vec{\tau}_1} \left[t_1^{\prime mn} + t_3^{\prime mn} e^{-i\vec{k} \cdot \vec{\xi}_1} + t_4^{\prime mn} \left(e^{i\vec{k} \cdot \vec{\xi}_2} + e^{i\vec{k} \cdot \vec{\xi}_3} \right) \right]; d_1^{mn}(\vec{k}) = e^{i\vec{k} \cdot \vec{\delta}_1} \left[t_1^{mn} + t_3^{mn} e^{-i\vec{k} \cdot \vec{\xi}_1} + t_4^{mn} \left(e^{i\vec{k} \cdot \vec{\xi}_2} + e^{i\vec{k} \cdot \vec{\xi}_3} \right) \right] \\ \tau_2^{mn}(\vec{k}) &= e^{i\vec{k} \cdot \vec{\tau}_2} \left[t_1^{\prime mn} + t_3^{\prime mn} e^{-i\vec{k} \cdot \vec{\xi}_2} + t_4^{\prime mn} \left(e^{i\vec{k} \cdot \vec{\xi}_3} + e^{i\vec{k} \cdot \vec{\xi}_1} \right) \right]; d_2^{mn}(\vec{k}) = e^{i\vec{k} \cdot \vec{\delta}_2} \left[t_1^{mn} + t_3^{mn} e^{-i\vec{k} \cdot \vec{\xi}_2} + t_4^{mn} \left(e^{i\vec{k} \cdot \vec{\xi}_3} + e^{i\vec{k} \cdot \vec{\xi}_1} \right) \right] \\ \tau_3^{mn}(\vec{k}) &= e^{i\vec{k} \cdot \vec{\tau}_3} \left[t_1^{\prime mn} + t_3^{\prime mn} e^{-i\vec{k} \cdot \vec{\xi}_3} + t_4^{\prime mn} \left(e^{i\vec{k} \cdot \vec{\xi}_1} + e^{i\vec{k} \cdot \vec{\xi}_2} \right) \right]; d_3^{mn}(\vec{k}) = e^{i\vec{k} \cdot \vec{\delta}_3} \left[t_1^{mn} + t_3^{mn} e^{-i\vec{k} \cdot \vec{\xi}_3} + t_4^{mn} \left(e^{i\vec{k} \cdot \vec{\xi}_1} + e^{i\vec{k} \cdot \vec{\xi}_2} \right) \right] \end{aligned} \quad (42)$$

Using the following unitary transformation one can separate the bilayer graphene Hamiltonian Eq. 35 into two decoupled single layer pseudo-graphene Hamiltonians, where one of them is decorated with the intercalant layer

$$H_D = Q_T^\dagger H_N(\vec{k}) Q_T = \left[\begin{array}{cc|c} h_0(\vec{k}) & \sqrt{2}h_{01}(\vec{k}) & 0 \\ \sqrt{2}h_{10}(\vec{k}) & H^+(\vec{k}) & 0 \\ \hline 0 & 0 & H^-(\vec{k}) \end{array} \right], \quad Q_T = \frac{1}{\sqrt{2}} \left(\begin{array}{c|cc} \sqrt{2} & 0 & 0 \\ \hline 0 & I_{6 \times 6} & I_{6 \times 6} \\ 0 & I_{6 \times 6} & -I_{6 \times 6} \end{array} \right). \quad (43)$$

Here $H^\pm = H_{11}(\vec{k}) \pm H_{12}$ in matrix notation is

$$H^\pm(\vec{k}) = H_{11}(\vec{k}) \pm H_{12}(\vec{k}) = \left(\begin{array}{ccc|ccc} \varepsilon_1^\pm(\vec{k}) & \beta^\pm(\vec{k}) & \gamma^\pm(\vec{k}) & \tau_1^\pm(\vec{k}) & d_2^\pm(\vec{k}) & d_3^\pm(\vec{k}) \\ \beta^{\pm*}(\vec{k}) & \varepsilon_1^\pm(\vec{k}) & \theta^\pm(\vec{k}) & d_2^\pm(\vec{k}) & \tau_3^\pm(\vec{k}) & d_1^\pm(\vec{k}) \\ \gamma^{\pm*}(\vec{k}) & \theta^{\pm*}(\vec{k}) & \varepsilon_1^\pm(\vec{k}) & d_3^\pm(\vec{k}) & d_1^\pm(\vec{k}) & \tau_2^\pm(\vec{k}) \\ \hline \tau_1^{\pm*}(\vec{k}) & d_2^{\pm*}(\vec{k}) & d_3^{\pm*}(\vec{k}) & \varepsilon_2^\pm(\vec{k}) & \beta^{\pm*}(\vec{k}) & \gamma^{\pm*}(\vec{k}) \\ d_2^{\pm*}(\vec{k}) & \tau_3^{\pm*}(\vec{k}) & d_1^{\pm*}(\vec{k}) & \beta^\pm(\vec{k}) & \varepsilon_2^\pm(\vec{k}) & \theta^{\pm*}(\vec{k}) \\ d_3^{\pm*}(\vec{k}) & d_1^{\pm*}(\vec{k}) & \tau_2^{\pm*}(\vec{k}) & \gamma^\pm(\vec{k}) & \theta^\pm(\vec{k}) & \varepsilon_2^\pm(\vec{k}) \end{array} \right) \quad (44)$$

in which \vec{k} -dependent on-site energies have been defined as $\varepsilon_1^\pm(\vec{k}) = \varepsilon_A - \mu_0 + \alpha^\pm(\vec{k})$ and $\varepsilon_2^\pm(\vec{k}) = \varepsilon_B - \mu_0 + \alpha^\pm(\vec{k})$. Also the following shorthand notation has been introduced

$$\begin{aligned} \alpha^\pm(\vec{k}) &= \left(\alpha^{11}(\vec{k}) \pm \alpha^{12}(\vec{k}) \right), \quad \beta^\pm(\vec{k}) = \left(\beta^{11}(\vec{k}) \pm \beta^{12}(\vec{k}) \right); \quad \tau_i^\pm(\vec{k}) = \left(\tau_i^{11}(\vec{k}) \pm \tau_i^{12}(\vec{k}) \right) \\ \gamma^\pm(\vec{k}) &= \left(\gamma^{11}(\vec{k}) \pm \gamma^{12}(\vec{k}) \right), \quad \theta^\pm(\vec{k}) = \left(\theta^{11}(\vec{k}) \pm \theta^{12}(\vec{k}) \right); \quad d_i^\pm(\vec{k}) = \left(d_i^{11}(\vec{k}) \pm d_i^{12}(\vec{k}) \right) \end{aligned} \quad (45)$$

Unitary transformation of Eq. 43 divides **thirteen** bands of intercalated bilayer graphene into, **six** and **seven** bands groups. Following the approach⁴¹ that has been applied to monolayer decorated graphene, an exact analytical solution of the six-band group can be found in general case. These bands are eigenvalues of H^- matrix and are not affected directly by the intercalant band.

In the special case of pristine bilayer graphene in which $\gamma^{\pm*}(\vec{k}) = \theta^\pm(\vec{k}) = \beta^\pm(\vec{k})$, $\varepsilon_1^\pm(\vec{k}) = \varepsilon_2^\pm(\vec{k})$ and $\tau_i^\pm(\vec{k}) = d_i^\pm(\vec{k})$, Eq. 44 easily can be diagonalized to find eigenvalues and also eigenvectors. The eigenvalues are given by

$$E_{\gamma,l}^\pm = \varepsilon_1^\pm(\vec{k}) + \beta^\pm(\vec{k}) + \beta^{\pm*}(\vec{k}) + (-1)^l t_1^\pm |\eta_0^\pm(\vec{k})| \quad (46)$$

$$E_{\alpha,l}^\pm = \varepsilon_1^\pm(\vec{k}) + e^{i2\pi/3} \beta^\pm(\vec{k}) + e^{-i2\pi/3} \beta^{\pm*}(\vec{k}) + (-1)^l t_1^\pm |\eta_1^\pm(\vec{k})| \quad (47)$$

$$E_{\beta,l}^{\pm} = \varepsilon_1^{\pm}(\vec{k}) + e^{-i2\pi/3}\beta^{\pm}(\vec{k}) + e^{i2\pi/3}\beta^{*\pm}(\vec{k}) + (-1)^l t_1^{\pm} |\eta_2^{\pm}(\vec{k})| \quad (48)$$

with eigenvectors are given by replacing m in the following equation with $m = 0, 1, 2$ respectively

$$\phi_{m,l}^{\pm}(\vec{k}) = \frac{1}{\sqrt{6}} [(u_m \quad u_m^* \quad 1) \quad (-1)^l \frac{\eta_m^{*\pm}}{|\eta_m^{\pm}|} (u_m^* \quad u_m \quad 1)]^T \quad (49)$$

wherein

$$\eta_m^{\pm}(\vec{k}) = d_2^{\pm}(\vec{k}) + u_m d_1^{\pm}(\vec{k}) + u_m^* d_3^{\pm}(\vec{k}); \quad u_m = e^{i2m\pi/3} \quad (50)$$

However, except at Γ point it is challenging (and unhelpful) to obtain an exact forms of the seven-bands group analytically. These bands are eigenvalues of the H_c^+ matrix, and analytic expressions for them can be obtained just in the particular case of no hopping between intercalant layer and graphene sheet, similar to the case for lithium intercalated bilayer graphene where intercalant band is empty (no Li-C hopping). In these cases nontrivial solutions are eigenvalues of H^+ matrix. Eigenvalues of H^- and H^+ matrices are given by⁴¹

$$E_{sh,m,l}^{\pm}(t_i, \vec{\xi}_i, \vec{k}) = \mu_m^{\pm}(\vec{k}) - \mu_o + \frac{1}{2} \left[\varepsilon_A + \varepsilon_B + (-1)^l \sqrt{(\varepsilon_A - \varepsilon_B)^2 + 4w_m^{\pm}(t_i, \vec{\xi}_i, \vec{k})} \right], \quad m = 1, 2, 3; \quad l = 1, 2 \quad (51)$$

in which \vec{k} dependent chemical potentials are defined as,

$$\mu_m^{\pm}(\vec{k}) = \alpha^{\pm}(\vec{k}) + u_m \Pi_0^{\pm}(t_2, \vec{\xi}_i, \vec{k}) + u_m^* \Pi_0^{\pm*}(t_2, \vec{\xi}_i, \vec{k}); \quad u_m = e^{2im\pi/3}. \quad (52)$$

The $\Pi_0^{\pm}(t_2, \vec{\xi}_i, \vec{k})$ function is introduced as

$$\Pi_0^{\pm}(t_2, \vec{\xi}_i, \vec{k}) = \left(\frac{c_0^{\pm}(t_2, \vec{\xi}_i, \vec{k})}{2} + i \sqrt{\left(\frac{c_1^{\pm}(t_2, \vec{\xi}_i, \vec{k})}{3} \right)^3 - \left(\frac{c_0^{\pm}(t_2, \vec{\xi}_i, \vec{k})}{2} \right)^2} \right)^{1/3}. \quad (53)$$

and, $c_0^{\pm}(t_2, \vec{\xi}_i, \vec{k}) = \gamma^{*\pm}(\vec{k})[\beta^{\pm}(\vec{k})\theta^{\pm}(\vec{k})] + \gamma^{\pm}(\vec{k})[\beta^{\pm}(\vec{k})\theta^{\pm}(\vec{k})]^*$ and $c_1^{\pm}(t_2, \vec{\xi}_i, \vec{k}) = |\beta^{\pm}(\vec{k})|^2 + |\theta^{\pm}(\vec{k})|^2 + |\gamma^{\pm}(\vec{k})|^2$. Also, $w_m^{\pm}(t_i, \vec{\xi}_i, \vec{k})$ are eigenvalues of the following matrices

$$G^{\pm} = \begin{pmatrix} \tau_1^{\pm}(\vec{k}) & d_2^{\pm}(\vec{k}) & d_3^{\pm}(\vec{k}) \\ d_2^{\pm}(\vec{k}) & \tau_3^{\pm}(\vec{k}) & d_1^{\pm}(\vec{k}) \\ d_3^{\pm}(\vec{k}) & d_1^{\pm}(\vec{k}) & \tau_1^{\pm}(\vec{k}) \end{pmatrix} \begin{pmatrix} \tau_1^{\pm*}(\vec{k}) & d_2^{\pm*}(\vec{k}) & d_3^{\pm*}(\vec{k}) \\ d_2^{\pm*}(\vec{k}) & \tau_3^{\pm*}(\vec{k}) & d_1^{\pm*}(\vec{k}) \\ d_3^{\pm*}(\vec{k}) & d_1^{\pm*}(\vec{k}) & \tau_1^{\pm*}(\vec{k}) \end{pmatrix}. \quad (54)$$

The eigenvalues can be obtained as

$$w_m^{\pm}(t_i, \vec{\xi}_i, \vec{k}) = \frac{C_2^{\pm}(t_i, \vec{\xi}_i, \vec{k})}{3} + u_m \Pi_1^{\pm}(t_i, \vec{\xi}_i, \vec{k}) + u_m^* \Pi_1^{\pm*}(t_i, \vec{\xi}_i, \vec{k}), \quad u_m = e^{2im\pi/3}; \quad m = 1, 2, 3. \quad (55)$$

wherein

$$\begin{aligned} C_2^{\pm}(t_i, \vec{\xi}_i, \vec{k}) &= G_{11}^{\pm} + G_{22}^{\pm} + G_{33}^{\pm} \\ C_1^{\pm}(t_i, \vec{\xi}_i, \vec{k}) &= |G_{12}^{\pm}|^2 + |G_{13}^{\pm}|^2 + |G_{23}^{\pm}|^2 - (G_{11}^{\pm} G_{22}^{\pm} + G_{11}^{\pm} G_{33}^{\pm} + G_{22}^{\pm} G_{33}^{\pm}) \\ C_0^{\pm}(t_i, \vec{\xi}_i, \vec{k}) &= G_{13}^{\pm} (G_{12}^{\pm} G_{23}^{\pm})^* + G_{13}^{\pm*} (G_{12}^{\pm} G_{23}^{\pm}) - G_{11}^{\pm} |G_{23}^{\pm}|^2 - G_{22}^{\pm} |G_{13}^{\pm}|^2 - G_{33}^{\pm} |G_{12}^{\pm}|^2 + G_{11}^{\pm} G_{22}^{\pm} G_{33}^{\pm} \end{aligned} \quad (56)$$

$$\begin{aligned} \Pi_1^{\pm}(t_i, \vec{\xi}_i, \vec{k}) &= \left(Q^{\pm}(t_i, \vec{\xi}_i, \vec{k}) + i \sqrt{P^{\pm}(t_i, \vec{\xi}_i, \vec{k})^3 - Q^{\pm}(t_i, \vec{\xi}_i, \vec{k})^2} \right)^{\frac{1}{3}} \\ Q^{\pm}(t_i, \vec{\xi}_i, \vec{k}) &= \frac{C_0^{\pm}(t_i, \vec{\xi}_i, \vec{k})}{2} + \frac{C_1^{\pm}(t_i, \vec{\xi}_i, \vec{k}) C_2^{\pm}(t_i, \vec{\xi}_i, \vec{k})}{6} + \frac{C_2^{\pm 3}(t_i, \vec{\xi}_i, \vec{k})}{27} \\ P^{\pm}(t_i, \vec{\xi}_i, \vec{k}) &= \frac{C_1^{\pm}(t_i, \vec{\xi}_i, \vec{k})}{3} + \frac{C_2^{\pm 2}(t_i, \vec{\xi}_i, \vec{k})}{9}. \end{aligned} \quad (57)$$

One can write the H_D matrix in H^\pm bases i. e. $H'_D = U^\dagger H_D U$,

$$H'_D = \left(\begin{array}{c|cccccc|cccccc} h_0(\vec{k}) & \gamma_1(\vec{k}) & \gamma_2(\vec{k}) & \gamma_3(\vec{k}) & \gamma_4(\vec{k}) & \gamma_5(\vec{k}) & \gamma_6(\vec{k}) & 0 & 0 & 0 & 0 & 0 & 0 \\ \hline \gamma_1^*(\vec{k}) & E_1^+(\vec{k}) & 0 & 0 & 0 & 0 & 0 & 0 & 0 & 0 & 0 & 0 & 0 \\ \gamma_2^*(\vec{k}) & 0 & E_2^+(\vec{k}) & 0 & 0 & 0 & 0 & 0 & 0 & 0 & 0 & 0 & 0 \\ \gamma_3^*(\vec{k}) & 0 & 0 & E_3^+(\vec{k}) & 0 & 0 & 0 & 0 & 0 & 0 & 0 & 0 & 0 \\ \gamma_4^*(\vec{k}) & 0 & 0 & 0 & E_4^+(\vec{k}) & 0 & 0 & 0 & 0 & 0 & 0 & 0 & 0 \\ \gamma_5^*(\vec{k}) & 0 & 0 & 0 & 0 & E_5^+(\vec{k}) & 0 & 0 & 0 & 0 & 0 & 0 & 0 \\ \gamma_6^*(\vec{k}) & 0 & 0 & 0 & 0 & 0 & E_6^+(\vec{k}) & 0 & 0 & 0 & 0 & 0 & 0 \\ \hline 0 & 0 & 0 & 0 & 0 & 0 & 0 & E_1^-(\vec{k}) & 0 & 0 & 0 & 0 & 0 \\ 0 & 0 & 0 & 0 & 0 & 0 & 0 & 0 & E_2^-(\vec{k}) & 0 & 0 & 0 & 0 \\ 0 & 0 & 0 & 0 & 0 & 0 & 0 & 0 & 0 & E_3^-(\vec{k}) & 0 & 0 & 0 \\ 0 & 0 & 0 & 0 & 0 & 0 & 0 & 0 & 0 & 0 & E_4^-(\vec{k}) & 0 & 0 \\ 0 & 0 & 0 & 0 & 0 & 0 & 0 & 0 & 0 & 0 & 0 & E_5^-(\vec{k}) & 0 \\ 0 & 0 & 0 & 0 & 0 & 0 & 0 & 0 & 0 & 0 & 0 & 0 & E_6^-(\vec{k}) \end{array} \right) \quad (58)$$

The upper left portion of Eq.58 can be obtained sufficiently well by perturbation theory.

XII. APPENDIX B: BOGOLIUBOV-DE GENNES TRANSFORMATION

The interacting Hamiltonian H_{su} in matrix representation is 14×14 matrix,

$$H_{su}(\vec{k}) = \sum_{\vec{k}} \hat{\Psi}^\dagger(\vec{k}) \begin{pmatrix} H_N(\vec{k}) & H_P(\vec{k}) \\ H_P^\dagger(\vec{k}) & -H_N^*(-\vec{k}) \end{pmatrix} \hat{\Psi}(\vec{k}) \quad (59)$$

where $\hat{\Psi}^\dagger(\vec{k}) = (\hat{c}_{0\uparrow}^\dagger(\vec{k}) \hat{c}_{1\uparrow}^\dagger(\vec{k}) \hat{c}_{2\uparrow}^\dagger(\vec{k}) \dots; \hat{c}_{12\uparrow}^\dagger(\vec{k}) \hat{c}_{0\downarrow}(-\vec{k}) \hat{c}_{1\downarrow}(-\vec{k}) \hat{c}_{2\downarrow}(-\vec{k}) \dots \hat{c}_{12\downarrow}(-\vec{k}))$. H_N is Hamiltonian of the normal state and H_P is the pair interaction matrix. The full matrix must be diagonalized to obtain the quasiparticle spectrum.

The mean field superconducting Hamiltonian of Eq. 1 in Nambu space is $\hat{H}_{su} = \sum_{\vec{k}} \hat{\Psi}^\dagger(\vec{k}) H_{su}(\vec{k}) \hat{\Psi}(\vec{k})$ where H_{su} in matrix representation is,

$$H_{su}(\vec{k}) = \begin{pmatrix} H_N(\vec{k}) & H_P(\vec{k}) \\ H_P^\dagger(\vec{k}) & -H_N^*(-\vec{k}) \end{pmatrix} = \left(\begin{array}{c|cc} \left(\begin{array}{c|cc} h_0(\vec{k}) & h_{01}(\vec{k}) & h_{02}(\vec{k}) \\ \hline h_{10}(\vec{k}) & H_{11}(\vec{k}) & H_{12}(\vec{k}) \\ h_{20}(\vec{k}) & H_{21}(\vec{k}) & H_{22}(\vec{k}) \end{array} \right) & \begin{bmatrix} 0 & 0 \\ 0 & H_{11}^P(\vec{k}) & H_{12}^P(\vec{k}) \\ 0 & H_{21}^P(\vec{k}) & H_{22}^P(\vec{k}) \end{bmatrix} \\ \hline \begin{bmatrix} 0 & 0 & 0 \\ 0 & H_{11}^P(\vec{k}) & H_{12}^P(\vec{k}) \\ 0 & H_{21}^P(\vec{k}) & H_{22}^P(\vec{k}) \end{bmatrix} & - \left(\begin{array}{c|cc} h_0(\vec{k}) & h_{01}(\vec{k}) & h_{02}(\vec{k}) \\ \hline h_{10}(\vec{k}) & H_{11}(\vec{k}) & H_{12}(\vec{k}) \\ h_{20}(\vec{k}) & H_{21}(\vec{k}) & H_{22}(\vec{k}) \end{array} \right) \end{array} \right) \quad (60)$$

and $\hat{\Psi}^\dagger(\vec{k}) = (\hat{c}_{0\uparrow}^\dagger(\vec{k}) \hat{c}_{1\uparrow}^\dagger(\vec{k}) \hat{c}_{2\uparrow}^\dagger(\vec{k}) \dots; \hat{c}_{12\uparrow}^\dagger(\vec{k}) \hat{c}_{0\downarrow}(-\vec{k}) \hat{c}_{1\downarrow}(-\vec{k}) \hat{c}_{2\downarrow}(-\vec{k}) \dots \hat{c}_{12\downarrow}(-\vec{k}))$ where $H_{11}(\vec{k}) = H_{22}(\vec{k})$. The interlayer pairing matrices are $H_{11}^P(\vec{k}) = H_{22}^P(\vec{k})$ and interlayer pairing matrices are $H_{12}^P(\vec{k}) = H_{21}^P(\vec{k})$. The pairing matrices are given by

$$H_{mn}^P(\vec{k}) = \left(\begin{array}{ccc|ccc} 0 & 0 & 0 & \Sigma_1^{mn}(\vec{k}) & \Delta_2^{mn}(\vec{k}) & \Pi_3^{mn}(\vec{k}) \\ 0 & 0 & 0 & \Pi_2^{mn}(\vec{k}) & \Sigma_3^{mn}(\vec{k}) & \Delta_1^{mn}(\vec{k}) \\ 0 & 0 & 0 & \Delta_3^{mn}(\vec{k}) & \Pi_1^{mn}(\vec{k}) & \Sigma_2^{mn}(\vec{k}) \\ \hline \Sigma_1^{mn*}(\vec{k}) & \Pi_2^*(\vec{k}) & \Delta_3^{mn*}(\vec{k}) & 0 & 0 & 0 \\ \Delta_2^{mn*}(\vec{k}) & \Sigma_3^{mn*}(\vec{k}) & \Pi_1^{mn*}(\vec{k}) & 0 & 0 & 0 \\ \Pi_3^{mn*}(\vec{k}) & \Delta_1^{mn*}(\vec{k}) & \Sigma_2^{mn*}(\vec{k}) & 0 & 0 & 0 \end{array} \right) \quad (61)$$

where m and n are layer index which can take 1 or 2. The order parameters accordingly in Fourier space are

$$\begin{aligned} \Sigma_l^{11}(\vec{k}) &= g_1 \Sigma_{l<ij>} e^{i\vec{k} \cdot \vec{\tau}_i}, & \Sigma_l^{12}(\vec{k}) &= g'_1 \Sigma'_{l<ij>} e^{i\vec{k} \cdot \vec{\tau}_i} \\ \Pi_l^{11}(\vec{k}) &= g_0 \Pi_{l<ij>} e^{i\vec{k} \cdot \vec{\delta}_i}, & \Pi_l^{12}(\vec{k}) &= g'_0 \Pi'_{l<ij>} e^{i\vec{k} \cdot \vec{\delta}_i} \\ \Delta_l^{11}(\vec{k}) &= g_0 \Delta_{l<ij>} e^{i\vec{k} \cdot \vec{\delta}_i}, & \Delta_l^{12}(\vec{k}) &= g'_0 \Delta'_{l<ij>} e^{i\vec{k} \cdot \vec{\delta}_i}, \quad l = 1, 2, 3. \end{aligned} \quad (62)$$

where $\langle ij \rangle$ subscript indicate nearest neighbor pairing amplitude in real space as illustrated in Fig.1. Introducing the following unitary transformation matrix,

$$\hat{H}_{su} = \sum_{\vec{k}} \hat{\Psi}^\dagger(\vec{k}) Q \left[Q^\dagger H_{su}(\vec{k}) Q \right] Q^\dagger \hat{\Psi}(\vec{k}) = \sum_{\vec{k}} \Lambda^\dagger(\vec{k}) H_s(\vec{k}) \Lambda(\vec{k}), \quad Q = \begin{pmatrix} Q_T(\vec{k}) & 0 \\ 0 & \hat{Q}_T^*(-\vec{k}) \end{pmatrix}, \quad (63)$$

one can transform Eq.63. Eq.60 can be transformed to the block diagonalize form

$$\hat{H}_{su} = \sum_{\vec{k}} \Lambda^\dagger(\vec{k}) \begin{pmatrix} H_{su}^+(\vec{k}) & 0 \\ 0 & H_{su}^-(\vec{k}) \end{pmatrix} \Lambda(\vec{k}) \quad (64)$$

in which

$$H_{su}^+(\vec{k}) = \begin{pmatrix} H_c^+(\vec{k}) & H_p^+(\vec{k}) \\ H_p^+(\vec{k}) & -H_c^+(\vec{k}) \end{pmatrix}_{14 \times 14}, \quad H_{su}^-(\vec{k}) = \begin{pmatrix} H^-(\vec{k}) & H_p^-(\vec{k}) \\ H_p^-(\vec{k}) & -H^-(\vec{k}) \end{pmatrix}_{12 \times 12} \quad (65)$$

and, $\Lambda^\dagger(\vec{k}) = \left([\hat{c}_{0\uparrow}^\dagger(\vec{k}) \hat{c}_{1\uparrow}^\dagger(\vec{k}) \dots \hat{c}_{6\uparrow}^\dagger(\vec{k}) \hat{c}_{0\downarrow}(-\vec{k}) \hat{c}_{1\downarrow}^\dagger(-\vec{k}) \dots \hat{c}_{6\downarrow}^\dagger(-\vec{k})] \quad [\hat{c}_{1\uparrow}^\dagger(\vec{k}) \hat{c}_{2\uparrow}^\dagger(\vec{k}) \dots \hat{c}_{6\uparrow}^\dagger(\vec{k}) \hat{c}_{1\downarrow}(-\vec{k}) \hat{c}_{2\downarrow}(-\vec{k}) \dots \hat{c}_{6\downarrow}(-\vec{k})] \right)$, where $\hat{c}_{m\sigma}^{(\pm)\dagger}(\vec{k}) = \frac{1}{\sqrt{2}}(\hat{c}_{m\sigma}^\dagger(\vec{k}) \pm \hat{c}_{m+6,\sigma}^\dagger(\vec{k}))$. New pairing matrices $H_p^+(\vec{k})$ and $H_p^-(\vec{k})$ are defined as,

$$H_p^+(\vec{k}) = \begin{pmatrix} 0 & 0 \\ 0 & H_p^{11}(\vec{k}) + H_p^{12}(\vec{k}) \end{pmatrix}, \quad H_p^-(\vec{k}) = \left(H_p^{11}(\vec{k}) - H_p^{12}(\vec{k}) \right). \quad (66)$$

From Eq. 64 it can be seen that the superconducting Hamiltonian H_{su} can be diagonalized into two decoupled new superconducting Hamiltonian H_{su}^+ and H_{su}^- . Thus electrons just can be paired within the seven bands sector H_c^+ or within the six bands sector H^- , without coupling between the sectors. Thus superconductivity in bilayer graphene can be interpreted as two decoupled monolayer graphene-like systems with independent behaviors.

XIII. APPENDIX C: TWO SUPERCONDUCTING GAP EQUATIONS

The linearized superconducting gap equation are obtained by minimizing the quasiparticle free energy with respect to the nearest neighbor order parameter, or equivalently with respect to Δ_\pm^α . The free energy of system is

$$F = F^+ + F^- + F_0 = -\frac{2}{\beta} \sum_{\vec{k}} \sum_{n=1}^{13} \ln \left[2 \cosh\left(\frac{E_n^Q}{2k_B T}\right) \right] + F_0, \quad F_0 = -2N \sum_{\alpha=1}^{18} J_\alpha (\Delta^\alpha)^2. \quad (67)$$

For F^+ the summation runs over $n = 1, \dots, 7$ giving $E_n^Q = E_{n,s}^{Q+}$; for F^- the summation takes $n = 8, \dots, 13$ values giving $E_n^Q = E_{n,s}^{Q-}$, with $E_{n,s}^{Q\pm}$ introduced in Eqs. 19 and 20.

Minimization of the free energy with respect to Δ_\pm^α gives

$$\Delta_{\langle ij \rangle}^\beta + \Delta'_{\langle ij \rangle}{}^\beta = -\frac{1}{N} \sum_{\alpha=1}^9 \left[\sum_{\vec{k}} \sum_{n=1}^7 \sum_{i=1}^7 \frac{\tanh\left(\frac{E_n^{Q+}}{2k_B T}\right)}{E_n^+(\vec{k}) + E_i^+(\vec{k})} \left(\Omega_{ni}^{+\alpha}(\vec{k}) \Omega_{ni}^{+\ast\beta}(\vec{k}) + \Omega_{ni}^{+\beta}(\vec{k}) \Omega_{ni}^{+\ast\alpha}(\vec{k}) \right) \right] \Delta_+^\alpha \equiv -\sum_{\alpha=1}^9 \Gamma_{\beta\alpha}^+ \Delta_+^\alpha. \quad (68)$$

giving independent gap equations for the seven bands odd-symmetry graphene-like Hamiltonian H_c^+ . Minimizing the free energy with respect to Δ_-^α gives

$$\Delta_{\langle ij \rangle}^\beta - \Delta'_{\langle ij \rangle}{}^\beta = -\frac{1}{N} \sum_{\alpha=1}^9 \left[\sum_{\vec{k}} \sum_{n=1}^6 \sum_{i=1}^6 \frac{\tanh\left(\frac{E_n^{Q-}}{2k_B T}\right)}{E_n^-(\vec{k}) + E_i^-(\vec{k})} \left(\Omega_{ni}^{-\alpha}(\vec{k}) \Omega_{ni}^{-\ast\beta}(\vec{k}) + \Omega_{ni}^{-\beta}(\vec{k}) \Omega_{ni}^{-\ast\alpha}(\vec{k}) \right) \right] \Delta_-^\alpha \equiv -\sum_{\alpha=1}^9 \Gamma_{\beta\alpha}^- \Delta_-^\alpha. \quad (69)$$

where Δ^α as illustrated in Fig.1(b) covers all possible nearest neighbor inter- and intra-layer C-C pairing amplitudes. Eqs. 76 and Eq. 69 in matrix form written as

$$\begin{bmatrix} A^\pm & B^\pm & B^\pm \\ B^\pm & C^\pm & D^\pm \\ B^\pm & D^\pm & C^\pm \end{bmatrix} \begin{pmatrix} g_1 \Sigma_i \pm g'_1 \Sigma'_i \\ g_0 \Pi_i \pm g'_0 \Pi'_i \\ g_0 \Delta_i \pm g'_0 \Delta'_i \end{pmatrix} = - \begin{pmatrix} \Sigma_i \pm \Sigma'_i \\ \Pi_i \pm \Pi'_i \\ \Delta_i \pm \Delta'_i \end{pmatrix}. \quad (70)$$

Equivalently, Eqs. 76 and 69 can be combined in the following non-Hermitian eigenvalue problem,

$$\begin{bmatrix} G^+ & \kappa_0 G^- \\ G^- & \kappa_0 G^+ \end{bmatrix} \begin{pmatrix} \Psi_\Delta \\ \Psi'_\Delta \end{pmatrix} = -\frac{1}{g_0} \begin{pmatrix} \Psi_\Delta \\ \Psi'_\Delta \end{pmatrix} \quad (71)$$

in which $\kappa_0 = \frac{g_0}{g'_0}$ and

$$G^\pm = \frac{1}{2} \begin{bmatrix} \kappa(A^+ \pm A^-) & \kappa(B^+ \pm B^-) & \kappa(B^+ \pm B^-) \\ (B^+ \pm B^-) & (C^+ \pm C^-) & (D^+ \pm D^-) \\ (B^+ \pm B^-) & (D^+ \pm D^-) & (C^+ \pm C^-) \end{bmatrix}, \quad \Psi_\Delta = \begin{pmatrix} g_1 V_1 \\ g_0 V_2 \\ g_0 V_3 \end{pmatrix}, \quad \Psi'_\Delta = \begin{pmatrix} g'_1 V'_1 \\ g'_0 V'_2 \\ g'_0 V'_3 \end{pmatrix}. \quad (72)$$

$\kappa = \frac{g_1}{g_0} = \frac{g'_1}{g'_0}$, $V_1^T = (\Sigma_1 \Sigma_2 \Sigma_3)$, $V_2^T = (\Pi_1 \Pi_2 \Pi_3)$, and $V_3^T = (\Delta_1 \Delta_2 \Delta_3)$. Also $V'_1{}^T = (\Sigma'_1 \Sigma'_2 \Sigma'_3)$, $V'_2{}^T = (\Pi'_1 \Pi'_2 \Pi'_3)$, and $V'_3{}^T = (\Delta'_1 \Delta'_2 \Delta'_3)$. Equation 71 is in fact the matrix representation of gap equation resulting from minimization of the free energy with respect to nearest neighbor order parameters instead of Δ_\pm^α , which can be solved to obtain the differing superconductivity phases and pairing interaction potentials.

In the limiting case $\kappa_0 \rightarrow 1$, the inter- and intra-layer pairing amplitudes in real space are equal, *i.e.* $g_0 = g'_0$ and $g_1 = g'_1$. This restriction makes the matrix gap equation hermitian and implies that band order parameters $\Delta_{mn}^\pm(\vec{k})$ can be interpreted physically as pairing of electrons in different bands with pairing interaction g_0^\pm . Just in this limit $\Delta_{mn}^\pm(\vec{k})$ is equal to the product of band Green function and g_0 ,

$$\Delta_{mn}^\pm(\vec{k}) = g_0^\pm \langle \hat{d}_m^{\pm\uparrow}(\vec{k}) \hat{d}_n^{\pm\downarrow}(\vec{k}) \rangle. \quad (73)$$

Here $\hat{d}_i^{\pm\sigma}(\vec{k}) = \sum_{m=1}^7 \mathcal{C}_m^{\pm*}(E_i(\vec{k})) \hat{c}_m^\sigma(\vec{k})$ annihilates an electron with spin σ in the i th six (odd) or seven (even) sector bands with energy $E_i^\pm(\vec{k})$. In this limit, Eq. 71 has two solutions $\Psi_\Delta = \Psi'_\Delta$ or $\Psi_\Delta = -\Psi'_\Delta$. The corresponding gap equations Eqs. 70 and 71 become decoupled gap equations corresponding to the even or odd sector of the graphene-like systems.

$$F^+ \Psi_\Delta = g_0^+ \Psi_\Delta, \quad F^- \Psi_\Delta = g_0^- \Psi_\Delta, \quad F^\pm = \begin{bmatrix} A^\pm & B^\pm & B^\pm \\ B^\pm & C^\pm & D^\pm \\ B^\pm & D^\pm & C^\pm \end{bmatrix} \quad (74)$$

XIV. APPENDIX D: FLAT BAND(S) SUPERCONDUCTIVITY

Mirror symmetry transformation rearranges the noninteracting Hamiltonian Eq. 8 as the direct sum of two single layer pseudo-graphene structures $\hat{H}_N = \hat{H}_N^+ \oplus \hat{H}_N^-$ (even sector (+ sign) and odd sector (- sign))

$$\hat{H}_N^+ = \sum_{ij\sigma} \sum_{\alpha,\beta=0}^6 t_{i\alpha\sigma,j\beta\sigma}^+ \hat{c}_{i\alpha\sigma}^{+\dagger} \hat{c}_{j\beta\sigma}^+; \quad \hat{H}_N^- = \sum_{ij\sigma} \sum_{\alpha,\beta=1}^6 t_{i\alpha\sigma,j\beta\sigma}^- \hat{c}_{i\alpha\sigma}^{-\dagger} \hat{c}_{j\beta\sigma}^- \quad (75)$$

with renormalized hopping integrals of the form $t_{i\alpha\sigma,j\beta\sigma}^\pm = t_{i\alpha\sigma,j\beta\sigma}^{inter} \pm t_{i\alpha\sigma,j\beta+6\sigma}^{intra}$. In the limit case of strong interlayer hopping wherein $t_{i\alpha\sigma,j\beta\sigma}^{inter} \rightarrow \pm t_{i\alpha\sigma,j\beta+6\sigma}^{intra}$ one can see that odd (or even) sector bandwidths completely become flat while the other sector bandwidth doubles. In this limit, thermal weight factor of Eq. 25 $\frac{\tanh(\frac{\beta E_i^\pm}{2})}{E_j^\pm(\vec{k}) + E_i^\pm(\vec{k})} \rightarrow \frac{\beta}{4}$ and so Γ matrix elements are given by

$$\Gamma_{\beta\alpha}^\pm = \frac{\beta}{4N} \sum_{\vec{k}} \sum_{ij} \left(\Omega_{ij}^{\pm\alpha}(\vec{k}) \Omega_{ji}^{\pm\beta}(\vec{k}) + \Omega_{ji}^{\pm\alpha}(\vec{k}) \Omega_{ij}^{\pm\beta}(\vec{k}) \right). \quad (76)$$

These elements are linked to the normal state Bloch coefficients via the $\Omega_{ij}^{\pm\beta}(\vec{k})$ factors that given by Eq. 21. For the case of pristine bilayer graphene, Eq. 76 can be determined analytically. In this limit, normal state Bloch coefficients are given by

$$[\mathcal{C}_1^\pm(E_{ml}) \dots \mathcal{C}_6^\pm(E_{ml})] = \frac{1}{\sqrt{6}} [(u_m \ u_m^* \ 1) \ (-1)^l e^{i\phi_m^\pm(\vec{k})} (u_m^* \ u_m \ 1)]; \quad u_m = e^{i2m\pi/3}, \quad m = 1, 2, 3 \ \& \ l = 1, 2 \quad (77)$$

wherein $e^{i\phi_m^\pm(\vec{k})} = \frac{\eta_m^{*\pm}}{|\eta_m^\pm|}$ and $\eta_m^\pm(\vec{k}) = d_2^\pm(\vec{k}) + u_m d_1^\pm(\vec{k}) + u_m^* d_3^\pm(\vec{k})$. $\Omega_{ij}^{\pm\beta}(\vec{k})$ factors can be calculated by substituting Bloch coefficients Eq. 77 in the Eq. 21. For instant one can show

$$\begin{aligned}
\Omega_{11}^{\pm 1}(\vec{k}) &= \Omega_{11}^{\pm 4}(\vec{k}) = \Omega_{11}^{\pm 7}(\vec{k}) = -\frac{1}{3}\cos(\vec{k}\cdot\vec{\delta}_1 - \phi_1^\pm(\vec{k})) \\
\Omega_{11}^{\pm 2}(\vec{k}) &= \Omega_{11}^{\pm 5}(\vec{k}) = \Omega_{11}^{\pm 8}(\vec{k}) = -\frac{1}{3}\cos(\vec{k}\cdot\vec{\delta}_2 - \phi_1^\pm(\vec{k})) \\
\Omega_{11}^{\pm 3}(\vec{k}) &= \Omega_{11}^{\pm 6}(\vec{k}) = \Omega_{11}^{\pm 9}(\vec{k}) = -\frac{1}{3}\cos(\vec{k}\cdot\vec{\delta}_3 - \phi_1^\pm(\vec{k})) \\
\Omega_{16}^{\pm 1}(\vec{k}) &= \Omega_{16}^{\pm 4}(\vec{k}) = \Omega_{16}^{\pm 7}(\vec{k}) = -\frac{i}{3}\sin(\vec{k}\cdot\vec{\delta}_1 - \phi_1^\pm(\vec{k})) \\
\Omega_{16}^{\pm 2}(\vec{k}) &= \Omega_{16}^{\pm 5}(\vec{k}) = \Omega_{16}^{\pm 8}(\vec{k}) = -\frac{i}{3}\sin(\vec{k}\cdot\vec{\delta}_2 - \phi_1^\pm(\vec{k})) \\
\Omega_{16}^{\pm 3}(\vec{k}) &= \Omega_{16}^{\pm 6}(\vec{k}) = \Omega_{16}^{\pm 9}(\vec{k}) = -\frac{i}{3}\sin(\vec{k}\cdot\vec{\delta}_3 - \phi_1^\pm(\vec{k}))
\end{aligned} \tag{78}$$

By calculating a large number of these factors and replacing them in the Eq. 76 one can obtain

$$\Gamma_{ij}^\pm = \beta_c \delta_{ij}; \quad g_0 = k_B T_c$$